



**HAL**  
open science

## Volcanism, jump and propagation on the Sheba ridge, eastern Gulf of Aden: segmentation evolution and implications for oceanic accretion processes

Elia d'Acremont, Sylvie Leroy, Marcia Maia, Pascal Gente, Julia Autin

### ► To cite this version:

Elia d'Acremont, Sylvie Leroy, Marcia Maia, Pascal Gente, Julia Autin. Volcanism, jump and propagation on the Sheba ridge, eastern Gulf of Aden: segmentation evolution and implications for oceanic accretion processes. *Geophysical Journal International*, 2010, 180 (2), pp.535-551. 10.1111/j.1365-246X.2009.04448.x . insu-00452873

**HAL Id: insu-00452873**

**<https://insu.hal.science/insu-00452873>**

Submitted on 7 Mar 2021

**HAL** is a multi-disciplinary open access archive for the deposit and dissemination of scientific research documents, whether they are published or not. The documents may come from teaching and research institutions in France or abroad, or from public or private research centers.

L'archive ouverte pluridisciplinaire **HAL**, est destinée au dépôt et à la diffusion de documents scientifiques de niveau recherche, publiés ou non, émanant des établissements d'enseignement et de recherche français ou étrangers, des laboratoires publics ou privés.

# Volcanism, jump and propagation on the Sheba ridge, eastern Gulf of Aden: segmentation evolution and implications for oceanic accretion processes

Elia d'Acremont,<sup>1</sup> Sylvie Leroy,<sup>1</sup> Marcia Maia,<sup>2,3</sup> Pascal Gente<sup>2,3</sup> and Julia Autin<sup>1</sup>

<sup>1</sup>Université Pierre et Marie Curie, Paris 06, ISTEP, CNRS-UMR 7193, Case 129, 4 place Jussieu, 75252 Paris Cedex 05, France.

E-mail: elia.dacremont@upmc.fr

<sup>2</sup>Université Européenne de Bretagne, France

<sup>3</sup>Université de Brest; CNRS, UMR6538 Domaines Océaniques, IUEM, Place Nicolas Copernic, 29280 Plouzané, France

Accepted 2009 November 6. Received 2009 November 6; in original form 2009 March 21

## SUMMARY

The rifting between Arabia and Somalia, which started around 35 Ma, was followed by oceanic accretion from at least 17.6 Ma leading to the formation of the present-day Gulf of Aden. Bathymetric, gravity and magnetic data from the Encens-Sheba cruise are used to constrain the structure and segmentation of the oceanic basin separating the conjugate continental margins in the eastern part of the Gulf of Aden between 51°E and 55.5°E. Data analysis reveals that the oceanic domain along this ridge section is divided into two distinct areas. The Eastern area is characterized by a shorter wavelength variation of the axial segmentation and an extremely thin oceanic crust. In the western segment, a thicker oceanic crust suggests a high melt supply. This supply is probably due to an off-axis melting anomaly located below the southern flank of the Sheba ridge, 75 km east of the major Alula-Fartak transform fault. This suggests that the axial morphology is produced by a combination of factors, including spreading rate, melt supply and the edge effect of the Alula-Fartak transform fault, as well as the proximity of the continental margin. The oceanic domains have undergone two distinct phases of accretion since the onset of seafloor spreading, with a shift around 11 Ma. At that time, the ridge jumped southwards, in response to the melting anomaly. Propagating ridges were triggered by the melting activity, and propagated both eastward and westward. The influence of the melting anomaly on the ridges decreased, stopping their propagation since less than 9 Ma. From that time up to the present, the N025°E-trending Socotra transform fault developed in association with the formation of the N115°E-trending segment #2. In recent times, a counter-clockwise rotation of the stress field associated with kinematic changes could explain the structural morphology of the Alula-Fartak and Socotra-Hadbeen fracture zones.

**Key words:** Gravity anomalies and Earth structure; Magnetic anomalies: modelling and interpretation; Mid-ocean ridge processes; Oceanic hotspots and intraplate volcanism; Oceanic transform and fracture zone processes; Crustal structure.

## 1 INTRODUCTION

In recent years, detailed geophysical and geological studies of spreading ridges and their flanks have emphasized the general variability of bathymetry and axial morphology, as well as the gravimetric and magnetic features (Fox & Grindlay 1991; Grindlay *et al.* 1992; Sempéré *et al.* 1993; Rommevaux *et al.* 1994; Gente *et al.* 1995; Maia & Gente 1998; Sauter *et al.* 2001).

The morphology and geophysical features of spreading centres vary with the rate of plate separation and/or magma supply. In contrast to the relative uniformity along fast-spreading ridges, slow-spreading ridges are highly segmented at varied intervals by both permanent transforms and non-rigid discontinuities. At slow spreading rates (full rate: 10–40 mm yr<sup>-1</sup>) the axis is marked by

a rift valley 1–3 km deep, while, at fast spreading rates (full rate: 90–170 mm yr<sup>-1</sup>) it is characterized by a seafloor elevation of several hundred metres (Macdonald 1982). The origin of this variability in topography, crustal thickness, gravity field and segment length is commonly attributed to differences in magma flux from the mantle (e.g. Lin *et al.* 1990; Thibaud *et al.* 1998; Niu *et al.* 2001; Supak *et al.* 2007). Especially, the average crustal thickness is strongly dependent on mantle properties and plate geometry, and spreading rate (Magde & Sparks 1997).

Several hypotheses have been proposed to explain the processes controlling the segmentation of a spreading centre and its evolution with time: (1) the absolute motion of the ridge over the underlying asthenosphere (Schouten *et al.* 1987; Supak *et al.* 2007), (2) the plate tectonic history or local parameters such as spreading rate

or magma supply (Schouten *et al.* 1985; Kuo & Forsyth 1988; Macdonald *et al.* 1991).

The eastern Gulf of Aden is a key area for investigating seafloor spreading processes and the evolution of segmentation in space and time from the continental margin to the present active ridge. The Gulf of Aden is a small oceanic basin with close conjugate margins allowing a complete geophysical investigation from ridge to rift. This paper presents geophysical data gathered during the Encens-Sheba cruise (Leroy *et al.* 2004) and also makes use of additional magnetic data acquired during the recent Encens Cruise (Leroy *et al.* 2009a). The swath coverage spans the area of seafloor spreading from the continental margins to the ridge axis. The data coverage allows us to study the structure of both the oceanic basin and the present active ridge. We therefore attempt (1) to describe the active ridge and present segmentation (2) to determine the crustal thickness of the oceanic domains and (3) to identify crustal discontinuities that serve to determine the development of segmentation from the ocean–continent transition to the active Sheba ridge. The general structure and tectonic evolution of the conjugate continental margins in relation to the onset of oceanic spreading were reported in d'Acremont *et al.* (2005, 2006). In this study, we focus on the oceanic basin between the Alula-Fartak Fracture Zone (AFFZ) and the Socotra-Hadbeen Fracture Zone (SHFZ), presenting a detailed analysis of bathymetric, magnetic and gravity data to constrain the evolution in terms of ridge geometry, segmentation and transform structure over time. We propose that anomalous volcanic activity may have an influence on the ridge jump and ridge propagation and, as a result, the accretion processes as well. We discuss the relationship of these processes with the associated changes in kinematics.

## 2 GEODYNAMIC SETTING

The Gulf of Aden is a young oceanic basin separating the Arabia and Somalia plates, with a N75°E-trending axis running obliquely to the N26°E opening direction (Fig. 1). It is bordered to the north and south by rifted margins, and to the west and east by the Afar triple junction and the Owen fracture zone, respectively. Continental rifting started 35 Ma (Roger *et al.* 1989), while the onset of oceanic

spreading is at 20 Ma in the easternmost part of the Gulf near the Owen Fracture zone (Fournier *et al.* 2008), it occurs at 17.6 Ma between the east of Socotra Island and the AFFZ (Leroy *et al.* 2004; d'Acremont *et al.* 2006; Leroy *et al.* 2009b) and 16 Ma in the west of the AFFZ (Leroy *et al.* 2009b). Since the early opening between the Arabia and the Somalia plates about 20 Ma, the Euler pole of rotation has remained close to the ridge axis. The full spreading rate is correlated with the distance to the Euler pole, currently located at 24.01°N 24.57°E, increasing from 1.6 cm yr<sup>-1</sup> in the west along N37°E to 2.34 cm yr<sup>-1</sup> in the east along N26°E (Fournier *et al.* 2001).

The Gulf of Aden can be divided into three domains. (1) The westernmost domain, between the Gulf of Tadjoura and the Shukra-El Sheik Fracture zone, influenced by the Afar hotspot, whose main activity is contemporaneous with the onset of rifting (Schilling 1973; Courtillot 1980; Ebinger & Hayward 1996; Menzies *et al.* 1997). This led to the formation of volcanic margins (Tard *et al.* 1991) up to the Shukra-El Sheik Fracture zone, which is assumed to mark a major change in the rheology of the lithosphere (Manighetti *et al.* 1998; Dauteuil *et al.* 2001; Hébert *et al.* 2001). (2) The central domain, between the Shukra-El Sheik Fracture zone and the AFFZ, corresponds to the transition between volcanic and non-volcanic continental margins (Tard *et al.* 1991). (3) The eastern domain between the AFFZ and Owen fracture zone separates the Aden ridge segment from the Sheba ridge segment (Tamsett & Searle 1990). Indeed, the Alula-Fartak transform fault (AFTF) shifts the Aden ridge farther north towards the Sheba ridge. The continental margins are segmented and, in the area between the ~N027°E-trending AFFZ and SHFZ, the segmentation is expressed by two transfer fault zones with right-lateral offset, accommodating the oblique deformation (Fig. 2, d'Acremont *et al.* 2005). These transfer zones define three N110°E-trending segments. The first evidence of oceanic spreading corresponds to the magnetic anomaly A5d and thus dates back to 17.6 Ma at least (Leroy *et al.* 2004; d'Acremont *et al.* 2005). Reconstruction of the spreading process suggests a complex non-uniform opening by an arc-like initiation of seafloor spreading in the ocean–continent transition. Crustal accretion initially occurred prior to spreading at low extension rates in a magmatic-limited environment with potential exhumed mantle in the eastern segments

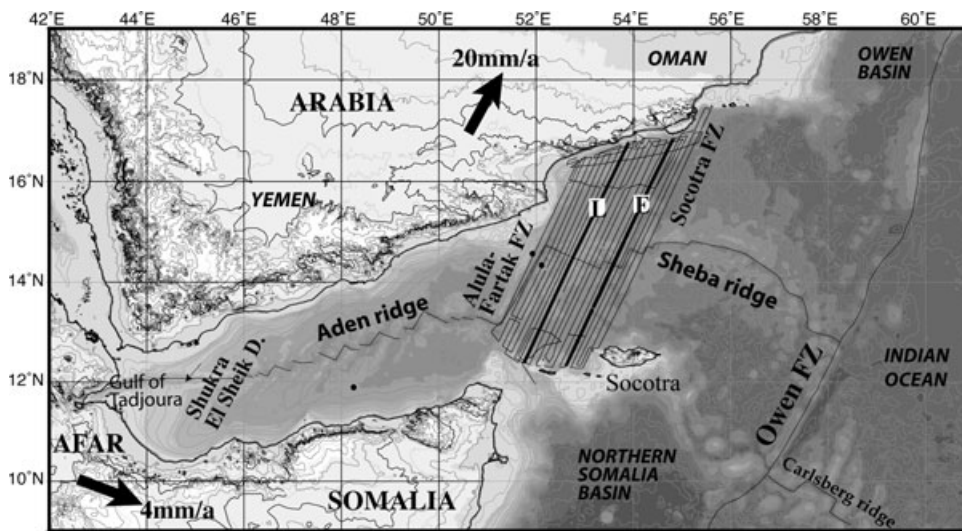


**Figure 1.** Bathymetric and topographic map of the Gulf of Aden area (Sandwell & Smith 1997). The solid lines represent the Encens-Sheba cruise track where bathymetry, magnetic and gravity data have been acquired. Bold lines correspond to the location of the seismic profiles. Black circles indicate DSDP drill holes of Leg 24 (Fisher *et al.* 1974). Solid arrows show the plate motion and the associated spreading rate (Jestin *et al.* 1994).

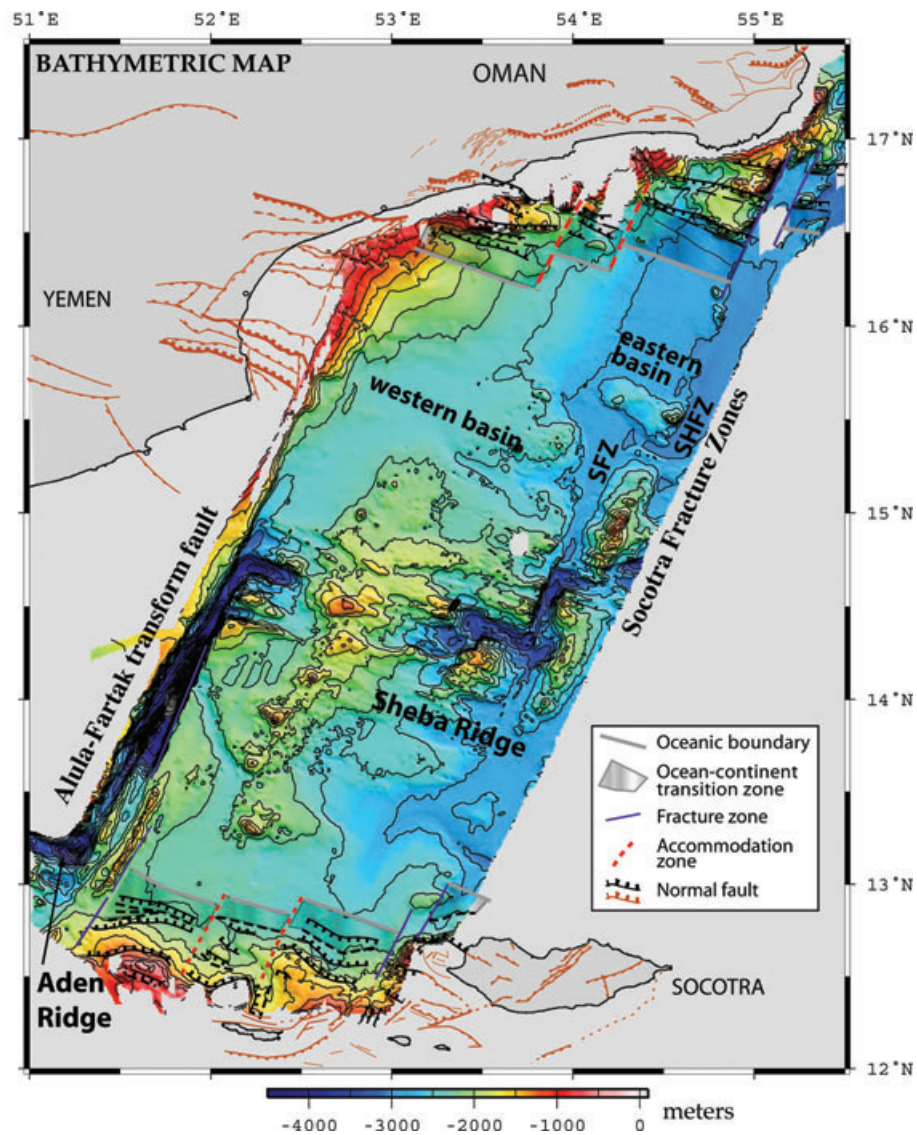


**Figure 2.** Multibeam bathymetry of the Encens-Sheba Cruise (Leroy *et al.* 2004; contour interval is 250 m). The structural interpretation on the offshore conjugate margins is after d'Acremont *et al.* (2005, 2006). On the onshore margins, the interpretation is after Beydoun & Bichan (1969), Platel & Roger (1989), Platel *et al.* (1992), Birse *et al.* (1997), Brannan *et al.* (1997), Lepvrier *et al.* (2002) and Bellahsen *et al.* (2006). SFZ: Socotra Fracture Zone; SHFZ: Socotra-Hadbeen Fracture Zone.

(d'Acremont *et al.* 2006). The early segmentation appears to be related to the continental margin segmentation (d'Acremont *et al.* 2006).

### 3 DATA

#### 3.1 Bathymetry and subsidence

A full bathymetry coverage of the study area was obtained with a Thomson Marconi Sonar on board *R/V Marion Dufresne* (Fig. 2, Leroy *et al.* 2004). A 100-m spaced bathymetric grid was obtained using the Caribes software developed by IFREMER (Leroy *et al.* 2000).

The bathymetric grid is corrected for the effect of seafloor subsidence with age. The subsidence of the seafloor is calculated using the relation  $S = 0.35 \sqrt{t}$ ; where  $t$  is the oceanic lithosphere age in Ma, obtained from the compiled isochron map and  $S$  is the

expected subsidence in km (Parsons & Sclater 1977). The residual bathymetry (corrected for subsidence with age) is obtained by subtracting this predicted subsidence from the bathymetric map. This result is used in the kinematic reconstruction to highlight possible relationships among older structures.

#### 3.2 Magnetic anomalies

During the Encens-Sheba cruise, a series of 19 across-axis profiles were recorded between the AFFZ and the SHFZ (Leroy *et al.* 2004; A to S; Fig. 1). To supplement this data, we used the new data set of the Encens cruise 2006 (Leroy *et al.* 2009a). In previous studies, Fleury (2001), Leroy *et al.* (2004) and d'Acremont *et al.* (2006) published selective or incomplete magnetic profiles of the Encens-Sheba cruise. The kinematic reconstructions presented below are based on the pole and angle of rotation obtained for the entire Gulf of Aden by Fleury (2001), using seafloor magnetic anomaly identification of new sources (Shackelton 1979 and ug78 Cruises).

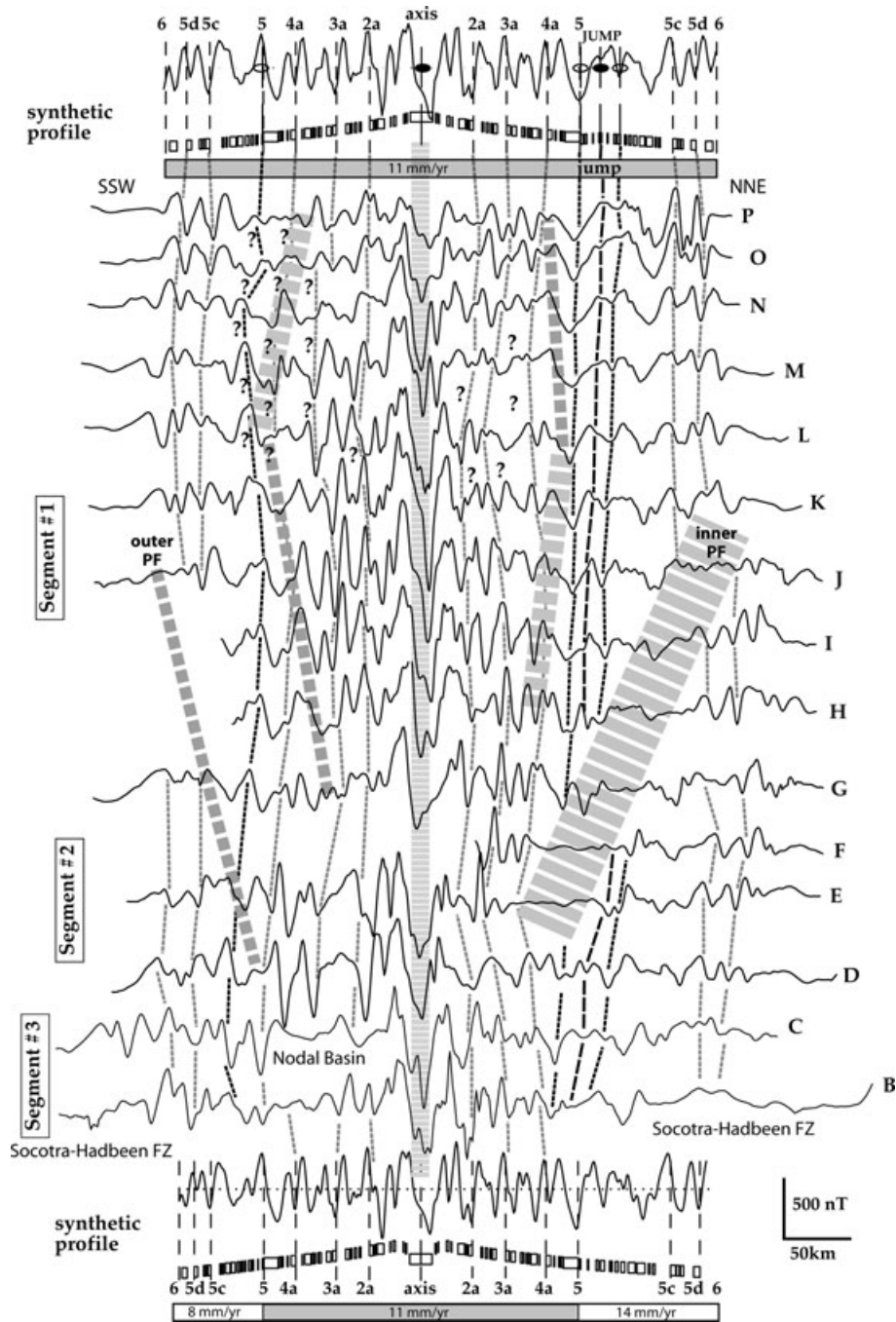


**Figure 3.** Identification of magnetic anomalies on profiles B to P. Profiles are projected onto the  $N206^{\circ}E$  direction. Top: synthetic profile including ridge jump at 11 Ma, 30 km southward, calculated for constant half spreading rate of  $11 \text{ mm yr}^{-1}$ . The black circles indicate the present-day and former ridge axes. The white and black circles correspond to the ridge jump. Bottom: synthetic profiles with asymmetric half spreading rates before 11 Ma. Grey zones correspond to the pseudo-faults: PF. Question marks indicate uncertain pickings.

With a mean spacing of 9 km between profiles, the whole data set provides sufficient resolution for a detailed and quantitative analysis of the evolution of the spreading ridge. The complete sequence of magnetic anomalies (A) from the central anomaly to A5d was identified on most of the profiles by comparing each magnetic profile with a 2-D forward block model (Fig. 3). These models are based on the magnetic reversal timescale of Cande & Kent (1995). However, several anomalies are difficult to recognize on the western profile, especially on the south flank close to the AFTF. In particular, a misfit is observed when matching the conjugate A5 picks. Because of this,

we need to modify the previous A5 identifications: we consider the northern flank picks as correct and, consequently, some picks are missing on the southern flank (profiles L to P, Fig. 3). The magnetic anomalies indicate an asymmetric spreading between A5 and A5c (Figs 3 and 4a). The best fit for the different profiles is obtained with a model involving a small ridge jump towards the south (30 km) just before the A5 epoch, and a half spreading rate of  $11 \text{ mm yr}^{-1}$  (Fig. 3). Another possible model involves asymmetric spreading between A5d to A5, with half spreading rates of  $14 \text{ mm yr}^{-1}$  for the northern flank of the ridge and  $8 \text{ mm yr}^{-1}$  for the southern flank

(Fig. 3). We have a preference for the jump model since it takes into account the fact that the anomalies between A5 to A5c are represented by two similar peaks and A5 is particularly large to the northwest. This ridge jump could probably explain why A5 is more difficult to recognize south of the ridge than to the north. Inspection of the shapes of the anomalies indicates the presence of pseudo-faults as well as a nodal basin and fracture zones, which are described in detail below (Fig. 3).

### 3.3 Gravity anomaly

Gravity data were acquired, at a 5 s sampling rate, with a Lacoste and Romberg S77 marine gravity meter. The data were processed for Eötvös and drift corrections and for removal of the gravity reference field (GRS80). After crossover errors, calculated for the data set, the final data STD error is 0.75 mGal. A continuous curvature gridding algorithm (Wessel & Smith 1998) is used to grid the corrected profiles. The relatively wide spacing between

the profiles (9–10 km) prevented the construction of a finer-scale free air anomaly (FAA) grid with a spatial resolution of ~20 km. We subtracted from the FAA the theoretical gravity effects of the water–sediment, sediment–crust and crust–mantle interfaces, thus obtaining the Mantle Bouguer Anomaly (MBA, Fig. 4b). The crustal thickness is assumed to be constant (6 km). The sedimentary thicknesses were compiled by using all available seismic reflection, multibeam bathymetric and magnetic data gathered between the AFFZ and SHFZ (Fig. 4a; d’Acremont *et al.* 2006). The densities of the sedimentary cover, the oceanic crust and the mantle are taken as 2.2, 2.75 and 3.3 g cm<sup>-3</sup>, respectively (e.g. Kuo & Forsyth 1988). The gravity effect of the model is computed with a fully 3-D multilayer method using a fast Fourier transform technique (Maia & Arkani-Hamed 2002). An infinite half-space model is used to calculate the gravity effect of the cooling lithosphere (Davis & Lister 1974). The thickness of the lithosphere is computed according to the thermal age. An age grid was computed from the magnetic anomaly picking and the lithosphere thermal diffusivity is taken as equal to

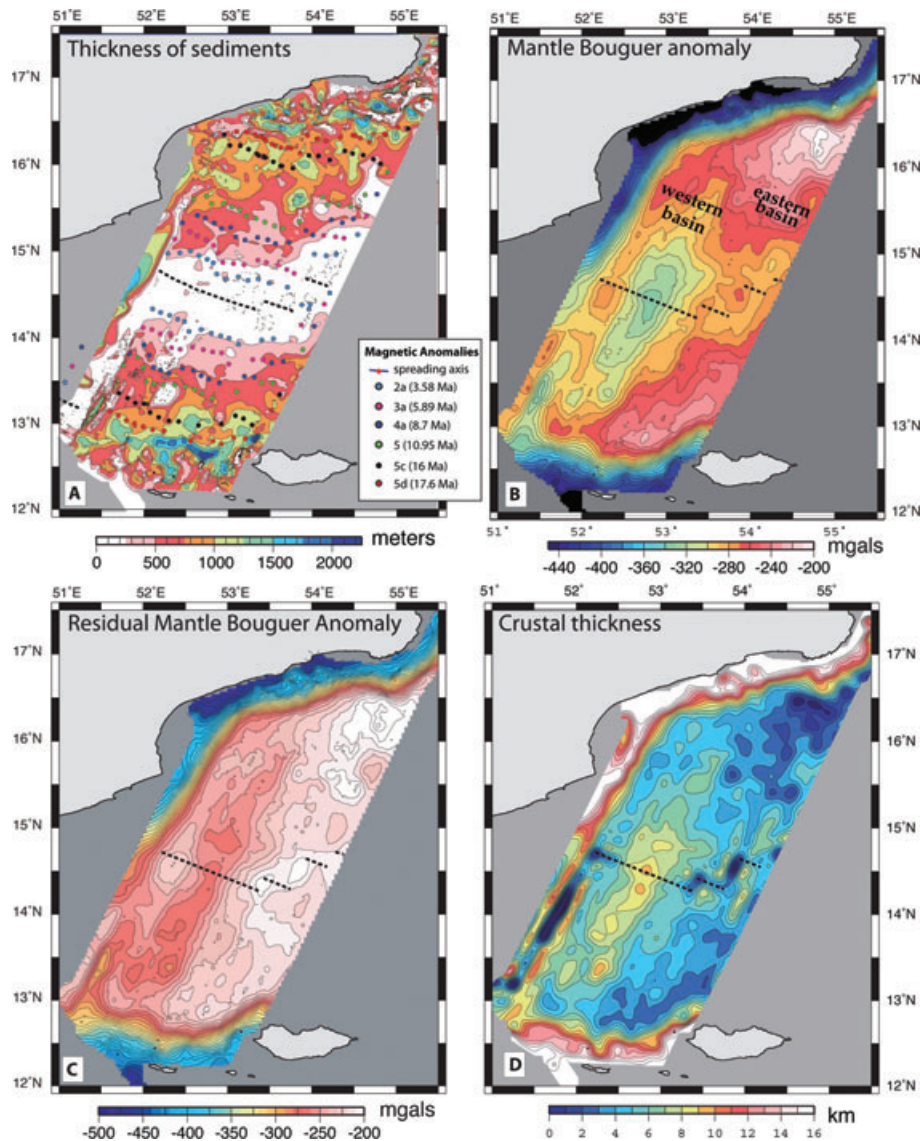


**Figure 4.** (a) Sediment thickness and the location of identified magnetic anomalies (contour interval is 250 m). (b) Mantle Bouguer Anomaly MBA (contour interval is 10 mGal). (c) Residual Mantle Bouguer Anomaly RMBA (contour interval is 10 mGal). (d) Crustal thickness obtained from downward continuation of the filtered gravity residuals (see text for explanations). The contour interval is 1 km. Dashed lines on the maps follow the Sheba ridge axis.

$10^{-6} \text{ m}^2 \text{ s}^{-1}$  (e.g. Phipps Morgan & Forsyth 1988; Sparks *et al.* 1993). This method is only suitable for the oceanic lithosphere. The edge effect of the continental lithosphere is not considered here, a laterally constant density is applied in the ocean–continent transition, even if non-realistic (d'Acremont *et al.* 2006).

The Residual Mantle Bouguer anomalies (RMBA), which are deviations from the assumed model, can be interpreted as resulting from variations in the crustal thickness and/or crust or mantle density (Kuo & Forsyth 1988; Lin *et al.* 1990). The RMBA amplitude ranges from  $-500$  to  $-200 \text{ mGal}$ , with the values tending to be significantly higher in the oceanic domain and lower near the continental margins (Fig. 4c). The highest values are observed over the northeastern part of the basin (Fig. 4c).

### 3.4 Crustal thickness

The RMBA corresponds to the component of the gravity field that cannot be explained by the predictable effect of seafloor topography, constant crustal thickness, or mantle density changes related to the cooling of the lithosphere. The residual anomaly is inverted here to determine the relative thickness of the crust (e.g. Morris & Detrick 1991; Fig. 4d; d'Acremont *et al.* 2006). The density contrast between mantle and crust (assuming densities of  $3.3$  and  $2.75 \text{ g cm}^{-3}$ , respectively) is similar to the value used for the gravity anomaly processing. The residual anomaly is continued downward to  $6 \text{ km}$  and added to the average seafloor depth. The Gaussian filtering used here leads to attenuation and/or removal of anomalies with wavelengths shorter than  $25\text{--}35 \text{ km}$ . The variations in crustal thickness are probably rather high since part of the gravity signal may also correspond to lateral variations in crustal or mantle den-

sity. Over the basin, the crustal thickness ranges from  $0$  to  $17 \text{ km}$  (Fig. 4d). The crust in the western basin is thicker than in the eastern basin. The northern and southern extremities of the eastern basin are characterized by an extremely thin crust.

## 4 STRUCTURE OF THE SHEBA RIDGE AND SURROUNDING BASIN

Two main domains of different roughness of bathymetry and contrasting RMBA appear between the first-order AFFZ and SHFZ (Figs 2 and 4c): (1) a rough seafloor, called the Western basin, characterized by volcanic domes and curved faults and (2) a faulted seafloor, called the Eastern basin, similar to that generally formed at slow-spreading centres. Three second-order ridge segments trending  $\sim\text{N}115^\circ\text{E}$  can be identified between longitude  $52^\circ\text{E}$  and  $54^\circ30'\text{E}$ , while another, called segment #4, trends  $\text{N}90^\circ\text{E}$  east of longitude  $54^\circ30'\text{E}$ . All four segments are associated with a well-defined rift valley or high neovolcanic zone (Figs 5 and 6) (Gente *et al.* 2001, 2003).

Average flank depths in the Eastern basin are deeper by about  $500 \text{ m}$  than in the Western basin (Fig. 2). On both sides of the axial valley, the rift valley walls show linear or curved abyssal ridges. These crests are asymmetrical, while, at the intersections between the segments and the discontinuity, the inside corners are higher. Between segments #1 and #2, the axis follows a series of two en-echelon basins located in a deep non-transform discontinuity, which offsets the axis by  $18 \text{ km}$  (Figs 5 and 6). By contrast, the offset between segments #2 and #3 is longer ( $45 \text{ km}$ ) and corresponds to the Socotra Transform Fault (STF). The study area is bounded to the

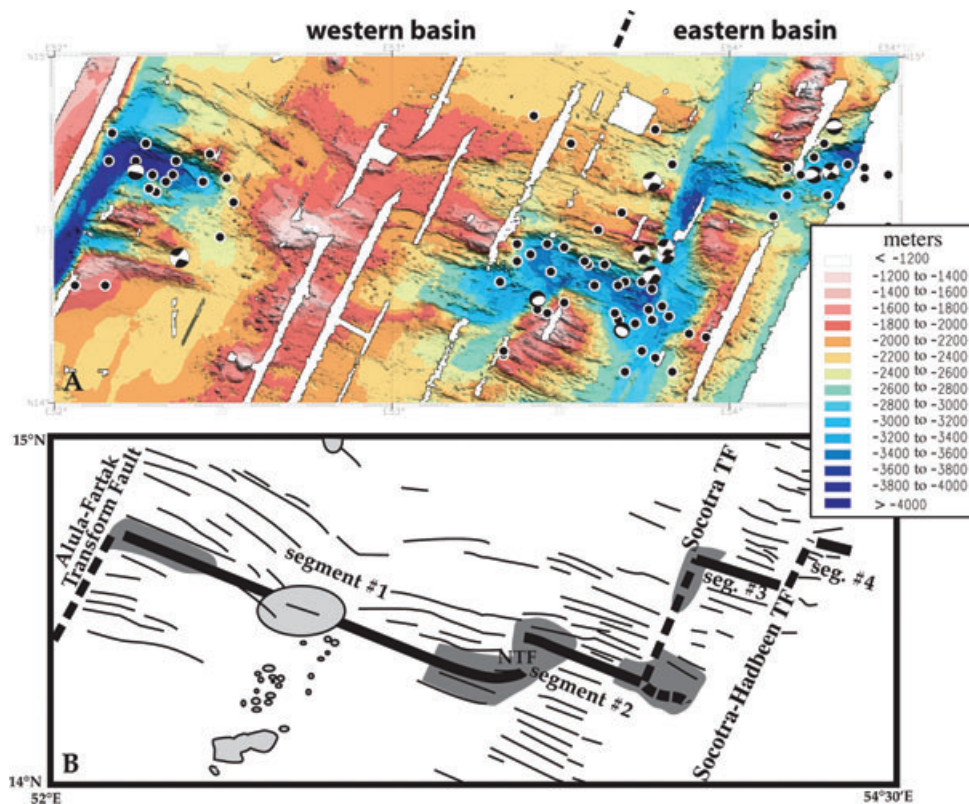


**Figure 5.** (a) Multibeam bathymetry of the Sheba Ridge with shallow seismicity since 1973 (focal depth  $< 50 \text{ km}$ ; magnitude  $> 2$ ; USGS/NEIC and Harvard database; CMT Focal mechanism represented on PDE location. (b) structural interpretation of the segmentation of the ridge. Light grey area corresponds to volcanoes, dark grey to nodal basins. NTF: non transform fault; TF: transform fault; seg.: segment.

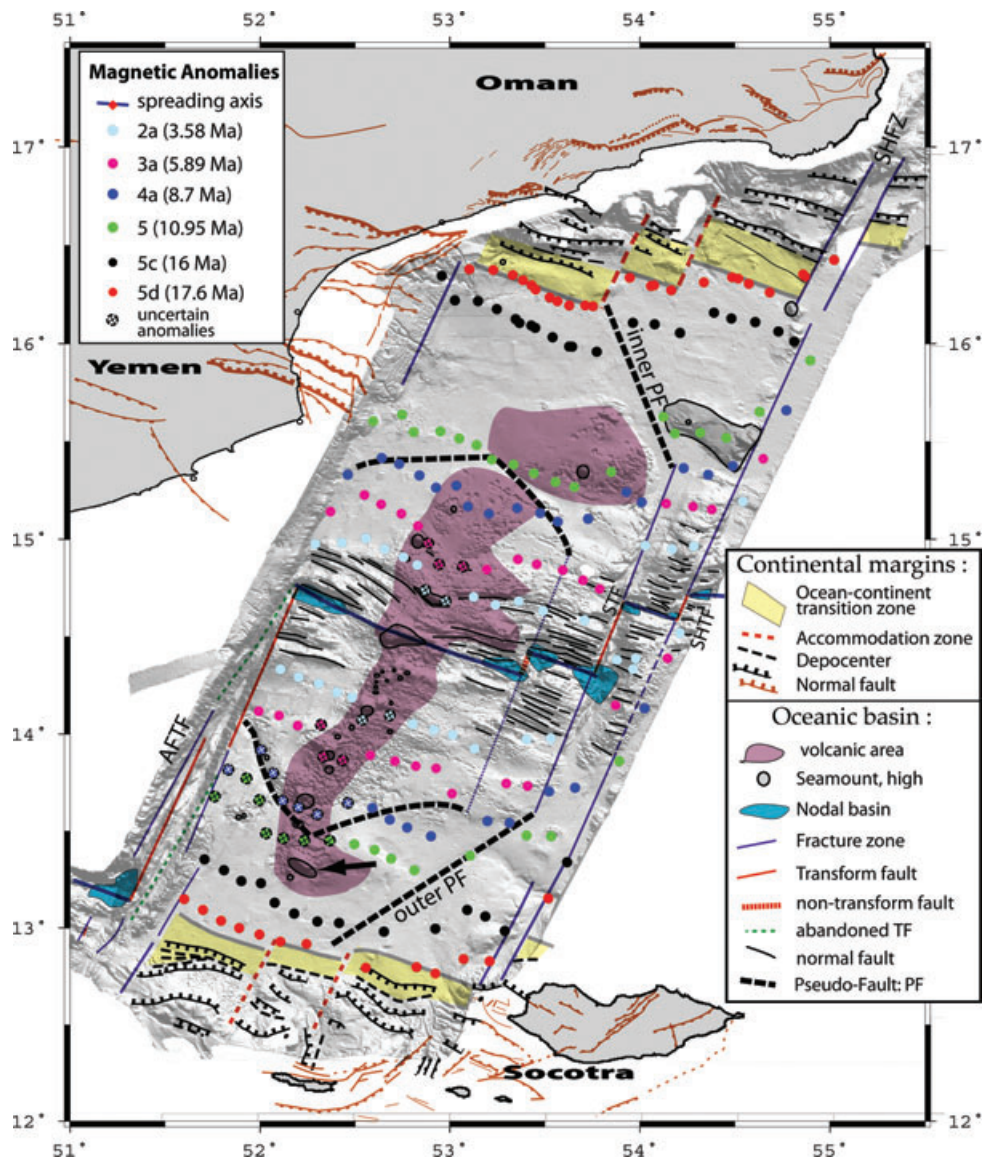


**Figure 6.** Structural map with magnetic anomalies cited in this study. Uncertain magnetic anomalies are indicated by crossed circles. On the offshore margins, the structural interpretation is according to d'Acremont *et al.* 2005, and, on the onshore margins, Beydoun & Bichan (1969), Platel & Roger (1989), Platel *et al.* (1992), Birse *et al.* (1997), Brannan *et al.* (1997), Lepvrier *et al.* (2002) and Bellahsen *et al.* (2006). AFTF: Alula-Fartak Transform Fault; STF: Socotra Transform Fault; SHTF: Socotra-Hadbeen Transform Fault; and SHFZ: Socotra-Hadbeen Fracture Zone. The arrow indicates the suggested melting anomaly (Leroy *et al.* 2009b).

east by the Socotra-Hadbeen Transform Fault (SHTF). The offset between segments #3 and #4 is about 10 km.

The first segment (#1), bounded to the west by the deep AFTF, is a 130-km-long spreading centre with a very shallow axis compared with normal slow-spreading ridges. The neovolcanic zone, located in the centre of the segment, is dominated by a 14-km diameter seamount rising to 1000 m below sea level (BSL). Many other small volcanoes are widespread on the flanks of the neovolcanic zone. At the ridge extremities, the tectonic scarps bound a nodal basin that is deeper and wider in the western part (4100 m BSL) than in the eastern part (3300 m BSL). The 40-km-long eastern segments (#2, #3 and #4) exhibit a more typical slow-spreading axial valley (3200–3600 m BSL). The axes of these segments are significantly deeper than the surrounding seafloor (~400 m). The eastern nodal basin of segment #2 cuts through the ridge crests of segment #3. The significant seismic activity in this basin is not restricted to the

deeper nodal basin, but persists on the eastern ridge crests (Fig. 5). The magnetic anomalies are strongly perturbed in this area (Fig. 3). This basin overlaps onto the southern ridge crests of segment #3 (Figs 5 and 6).

The bathymetric and crustal thickness maps and the magnetic anomalies reveal that the west and east domains are separated by a wide V-shaped boundary (Fig. 6), which is characterized by minimum crustal values and disturbed magnetic anomalies, pointing towards the SE (Figs 3, 4d and 7). The V-shaped trend defines the eastern end of segments #1 and #2 from A5d to A4a, and indicates an eastward propagation, increasing in length from 90 to 175 km (Fig. 6). This V-shaped boundary defines two pseudo-fault zones. The broad inner pseudo-fault observed on the magnetic data corresponds to the zone of transferred lithosphere defined by low-amplitude magnetic anomalies (Fig. 3; Briais *et al.* 2002).

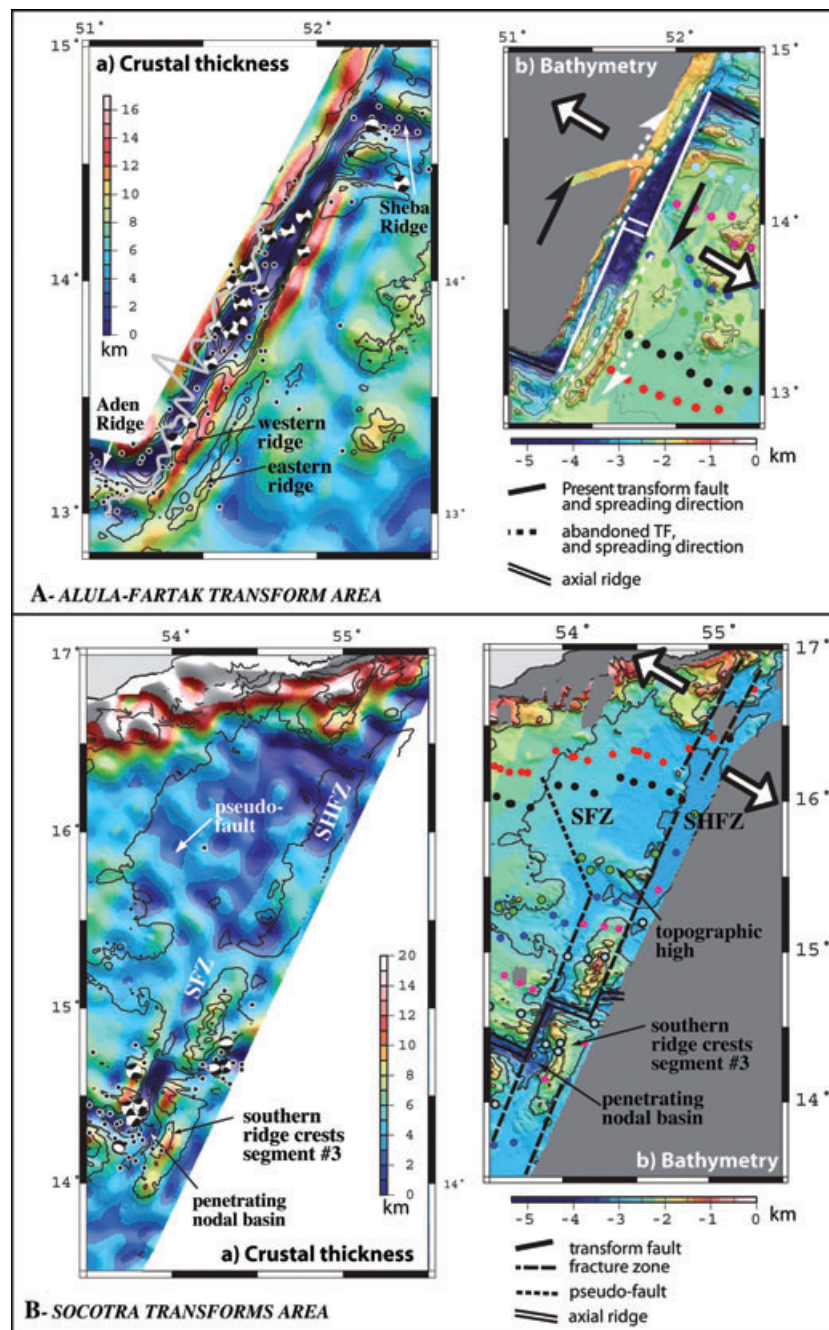


**Figure 7.** (A) Alula-Fartak Transform Fault: (a) crustal thickness map, with superimposed bathymetric contours (contour interval 500 m). Magnetic profile S is plotted along the ship's track as a grey line. The shallow seismicity is plotted since 1973 (focal depth <50 km; magnitude >2; USGS/NEIC and Harvard database; CMT Focal mechanisms represented on PDE location). (b) Cartoon based on bathymetric map illustrating the counter-clockwise change in spreading direction, which produces extension along the AFTF. A distensive component (open arrows) is already present at the onset of spreading direction change. A new spreading direction occurs immediately after the onset of plate motion change (continuous arrows). Flexural transverse ridges are formed subsequent to the opening episode and the abandonment of transform fault traces. (B) The Socotra and Socotra-Hadbeen Transforms and fracture zones: (a) crustal thickness map, with superimposed bathymetric contours (contour interval 500 m). The shallow seismicity is plotted since 1973 (focal depth <50 km; magnitude >2; USGS/NEIC and Harvard database; CMT Focal mechanisms represented on PDE location). (b) Cartoon based on bathymetric map illustrating the development of segmentation on the two transform faults. See Fig. 5 for legend concerning magnetic anomalies.

Moreover, two additional V-shaped boundaries are observed on the bathymetric map covering segment #1 (Figs 2 and 6). The more pronounced inner pseudo-fault zone corresponds to a distinct N150°E-trending topographic low at 2400 m BSL, which runs up against the AFTF at 14°N. The magnetic anomalies are perturbed

close to this basin (from A5 to A4a, Fig. 3). The RMBA and crustal thickness maps reveal variations of thickness and/or density in the crust or mantle. The two divergent V-shaped zones join in the middle of segment #1 close to A5, where the bathymetric and crustal thickness maps indicate a topographic low and a thinner crust,

respectively (Figs 4d and 6). The tips of the two conjugate pseudo-faults define the eastern and western ends of segment #1 from A5 to A4a, and indicate simultaneous and fast eastward–westward propagation directions on this microplate.

## 5 THE ALULA-FARTAK AND SOCOTRA-HADBEEN FRACTURES ZONES

The mean directions of the strike-slip earthquake slip vectors along the AFTF and STF are  $N025^{\circ}E \pm 5^{\circ}$  (DeMets *et al.* 1990; Tamsett & Searle 1990; DeMets *et al.* 1994; Fournier *et al.* 2001). The AFTF running across the entrance of the Gulf of Aden is the longest transform in this area (Fig. 1). The length of the AFTF, as defined by the distance between the offset of the Aden and Sheba axes, is about 180 km (Fig. 6; (Tamsett & Searle 1990). From east to west, the AFTF transforms the Sheba ridge to the Aden ridge in the vicinity of the southern continental margin at the ocean–continent transition, dated at 20 Ma (d'Acromont *et al.* 2005; Fig. 2). The thermal structure of the AFTF is strongly controlled or restricted by the continental lithosphere on either side. The lithospheric age contrast across the transform fault is 20 Ma at the ridge–transform intersections. The width of the transform zone is variable along strike, and ranges approximately from 10 km at the northern end to 30 km at the southern end (Fig. 7a). The deepest sounding in the transform valley (5350 m) occurs at around  $14^{\circ}N$  latitude (Fig. 7Ab). This part of the transform valley is notably asymmetric in cross section, the eastern wall being considerably steeper than the western wall (Fig. 7a; Tamsett & Searle 1990).

On the southeastern flank of the AFTF, a series of two ridges run subparallel to the transform fault zone (Fig. 7a). These 70-km-long parallel ridges (western and eastern) are flanked on the west along all their length by two elongated troughs. In the central part of the transform fault, the two elongated troughs join at around  $14^{\circ}N$  latitude (Fig. 7Ab). The 4000-m-deep inner basin of the Aden ridge bounds the western trough farther south. The eastern ridge is more prominent and shallower than the median ridge (1500 and 1900 m BSL, respectively). The two linear ridges are oriented parallel to the regional trend of the fracture zones, except for the southern part, where the eastern ridge and trough become oblique to the strike of the transform fault. These linear ridges rise above the surrounding seafloor and create anomalously shallow topography, and are thought to be composed predominantly of serpentinized ultramafic rocks (Bonatti 1978; Fox & Gallo 1984; Cannat 1993; Tucholke & Lin 1994; Escartin & Cannat 1999). Vertical tectonic activity could also be associated with the uprise of magmas following channelways produced by faulting (Menard & Atwater 1969). Gravity results show that the flanking ridges actually correspond to different crustal thicknesses (Fig. 7Aa): a mass excess with thin (or high density) crust on the eastern ridge (6–8 km thick) and mass deficits with thick (or low density) crust on the western ridge (13–15 km thick). The slight crustal thickening beneath the eastern ridge may be indicative of a high degree of serpentinization (Potts *et al.* 1986), but the eastern flanking ridge is punctuated by small closed-contour highs that are typically characteristic of volcanic structures. The uplift of the ridges could be explained by a flexure of the lithosphere and regional isostatic compensation (Potts *et al.* 1986; Tamsett & Searle 1990; Lonsdale 1994; Pockalny *et al.* 1996, 1997; Pockalny 1997).

Along the AFTF, the focal mechanisms indicate a present-day dextral strike-slip motion along a  $N25^{\circ}E$ -trending vertical fault

plane (Fig. 7Aa). At the southern end of the AFTF, tectonic activity is concentrated in the thin sediments of the western valley rather than in the thick sediments of the eastern valley (Laughton & Tramontini 1969; Cochran 1982; Tamsett & Searle 1990). Seismicity in the AFTF provides evidence for present-day active faulting located in the western valley (Fig. 7Aa). Oblique normal faults have been identified on the western wall of the AFTF, where they are interpreted as Riedel shears (Tamsett & Searle 1990).

The Socotra Fracture Zone is bounded to the north by a topographic high trending  $\sim N115^{\circ}$  associated with A5 (Figs 6 and 7Bb). The inner pseudo-fault, striking towards the SE, meets the palaeo-ridge (A4a) near  $54^{\circ}15'E$  and  $15^{\circ}15'N$  (Figs 6 and 7). Ultimately, the spreading ridge segmentation seems to be stable along the STF trend from A4a to A1 (Figs 6 and 7). A 25 km-wide valley defines the northern SHFZ. This valley, about 2900 m BSL, is markedly asymmetrical, with a western wall considerably steeper than the eastern wall (Fig. 7). The SHFZ seems continuous from the present transform up to the edge of the conjugate continental margins, except on the southern part of segment #3 where the ridge crests are shifted eastward due to the penetrating deep nodal basin (Fig. 7Bb). The SHFZ has two different directions: one parallel to the regional trend of present-day extensional motion from A5c–A5 to A1 ( $N025^{\circ}E$ ), and another oblique to this strike ( $N030^{\circ}E$ ) observed on the northern edge flank (Fig. 7Bb).

## 6 SEGMENT #1 ATYPICAL OF A SLOW SPREADING RIDGE

On segment #1 (western basin), there is a major morphological contrast between the central part and its extremities (Figs 2, 5 and 6). The abyssal volcanic hills, located in the centre of segment #1, have a relief of 3000 m and extend perpendicular to the active ridge. In the central part, there are almost no fault scarps. The segment extremities contain grabens parallel to the axial rift, which are bounded by topographic highs. The major fault scarps tend to propagate towards the centre of the segment while being curved. Thus, the walls are narrower on each side of the axis. This basin has a rougher seafloor fabric than the eastern basin, with many roughly circular volcanic cones, typically 500–600 m in height (Figs 2 and 5). This volcanic area is more extensive on the southern than on the northern flank. This shallow feature does not continue at depth, as confirmed by the lack of buried volcanic seamounts to the north (Fig. 8, profile E).

The bathymetric data fit very well with the gravimetric data in terms of segmentation. Segment #1 is marked by a negative Residual Mantle Bouguer Anomaly (RMBA) elongated in the spreading direction (SSW–NNE) (at the ridge axis  $\Delta MBA = 50$  mGal; Figs 4c and 9). The segment extremities are correlated with positive anomalies. The eastern segments are defined by negative RMBA of lower amplitude. The most negative RMBA is not centred on the ridge axis as usually observed at slow-spreading centres (Schouten *et al.* 1985; Kuo & Forsyth 1988; Lin *et al.* 1990; Rommevaux *et al.* 1994; Detrick *et al.* 1995), but is located in the southern area at latitude  $N13^{\circ}20'$  (Figs 4c and 6). We can interpret these negative residuals as due to a thickened crust or to lower densities in the crust and mantle.

From the ocean–continent transition to the active ridge, the crust inferred from gravity data is thinner in the eastern than in the western domain (Fig. 8). Segment #1 has an average oceanic thickness of about 8 km, while the crust of segments less affected by magmatic activity (#2, #3 and #4) is 4–5 km thick. For the two distinct domains,

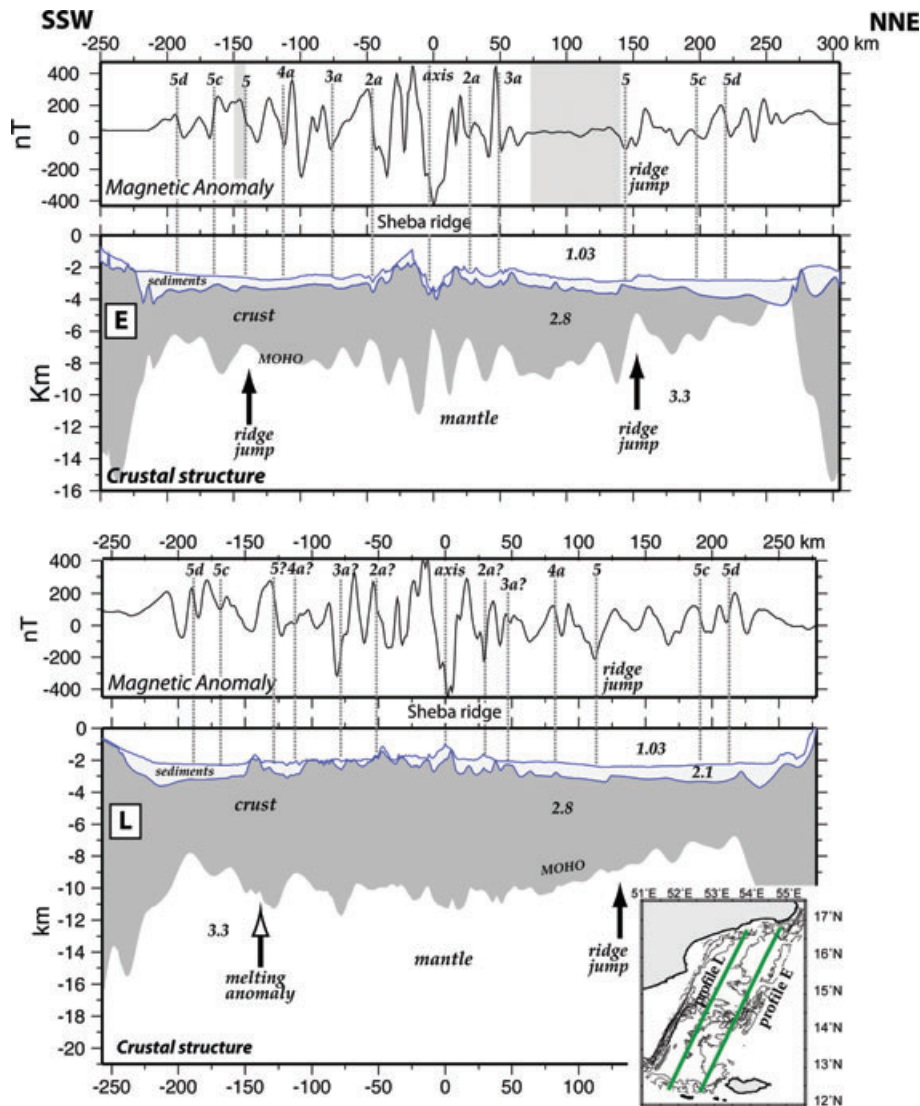


**Figure 8.** Computed magnetic model, with across-axis depth and magnetic profiles L and E. Profile locations are shown in the inset map. Across-axis magnetic anomalies profiles and profiles with bathymetry, depth to basement and Moho in km. Distances in km from the southwestern end-point of the profiles. The thick grey vertical lines indicate the location of pseudo-faults. Numbers on depth profiles indicate density values; the numbers refer to magnetic anomalies specified on the magnetic anomaly profiles.

there is a length and thickness asymmetry between the north and south flanks, with a shorter and thinner north flank, extending from A5 to the ocean–continent transition. The thickest crust on the oceanic domain is located above the southernmost volcanic dome of segment #1 (latitude N13°20'; Fig. 4d).

From the onset of spreading until present, the melt supply to segment #1 is anomalously high in comparison with the eastern segments. The long-wavelength negative RMBA may reflect more abundant magmatism than in the surrounding areas. In the volcanic area, the magnetic anomalies are disturbed in the southern flank along profiles K to P from A5c to A3a, consistent with the formation of seamount chains far from the axis (Figs 3 and 6). No seismicity is recorded. These results support the presence of an off-axis melting anomaly or a focused magmatic source located south of the ridge at latitude N13°20', which feeds the segment #1 ridge axis.

Thibaud *et al.* (1998) have determined relationships between gravity anomalies, axial topographic and length variations by synthesizing a large number of segments of the slow-spreading Mid-Atlantic-Ridge (MAR). In Fig. 9, we summarize these data from

MAR, while also introducing the data from segments #1 and #2 of this study. The length of the MAR segments varies from 11 to 90 km, with an average around 50 km.  $\Delta$ MBA varies from 3 to 45 mGal, with an average around 18 mGal. The axial depth relief corresponds to the variations of depth between the centre of the segment and an average depth between the two ends. It varies from 100 to 1500 m. Thibaud *et al.* (1998) observed two main types of segments: (1) the typical 'colder' slow-spreading MAR segments display a rough axial morphology with a deep, wide and well-defined rift valley, a low  $\Delta$ MBA and a short length. (2) The 'hotter' segment is characterized by a smooth axial morphology, a well-defined shallow inner valley, high  $\Delta$ MBA and a greater length. In our study, segment #2 is strongly correlated with 'colder' MAR values:  $\Delta$ MBA = 15 mGal, segment length = 40 km and variation in axial depth relief:  $\Delta$ R = 400 m (Fig. 9). While segment #1 is closest to the "hotter" type signatures, it falls outside Thibaud *et al.*'s data set:  $\Delta$ MBA = 50 mGal, segment length = 130 km and variation in axial depth relief:  $\Delta$ R = 3000 m (Fig. 9). These characteristics suggest that segment #1 is an end-member representative

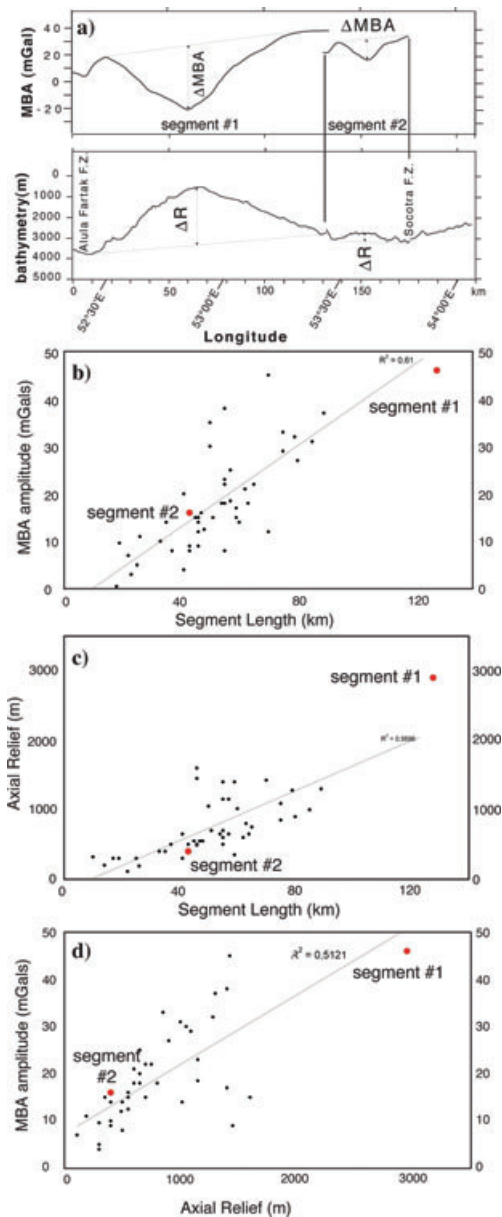


**Figure 9.** (a) MBA and bathymetric profiles along ridge axis in between AFTF and SHTF. (b–d). Comparison between study area (segment #1 and segment #2) and Mid-Atlantic Ridge (Thibaud *et al.* 1998): relationships between  $\Delta$ MBA, axial depth relief and segment length. Plots of segment length versus (b)  $\Delta$ MBA and (c) axial depth relief. Plot of axial depth relief versus (d)  $\Delta$ MBA.

of slow-spreading segments with ‘hotter-large-melt supply’ (Gente *et al.* 2003).

## 7 DISCUSSION: SPATIAL AND TEMPORAL EVOLUTION OF THE SEGMENTATION

### 7.1 Ridge jump and propagation

The melt supply to segment #1 is anomalously high in comparison with the eastern segments (Figs 9b, c and d). This is corroborated by its anomalously shallow axial depth, its anomalously high  $\Delta$ MBA

and an unusual chain of seamounts aligned in the spreading direction (SSW–NNE) and focused at 75-km east of the AFTF over the past 11 Ma. Compared with typical slow-spreading ridges, segment #1 exhibits features that are typical of ridge-hotspot interaction, with unusually high values of segment length, axial depth relief and  $\Delta$ MBA (Fig. 9).

However, the abrupt contrast observed between the western and eastern basin in the study area could be explained by rift-induced secondary mantle convection driven by thicker western margin lithosphere. This is the case in the Woodlark Basin, where such a mechanism significantly affects the young ocean basin in a way, which resembles increased spreading rate (Martinez *et al.* 1999). In this part of the Gulf of Aden, however, both eastern and western segments have similar tectonic history and degrees of stretching. Moreover, similar features (elongated seamount chain and negative RMBA) have been recorded across other accretion segments (such as segment OH1, Mid-Atlantic Ridge), where they are interpreted as a consequence of the cold edge effect of the Oceanographer fracture zone (Hooft *et al.* 2000; Rabain *et al.* 2001). The steep mantle isotherms due to the presence of the Oceanographer fracture zone would lead to a focusing (concentration or enhancement) of melting at the centre of the segment. Thus, the AFTF and the present-day geometry of the nearby continental margins could have a similar kind of edge effects on the segment #1 melt supply.

However, although the most negative gravity anomaly is usually centred below the active ridge, in our case the most negative RMBA of segment #1 is located on the southern flank at  $13^{\circ}20'N$  latitude (Fig. 4c). The magnetic anomalies are disturbed around the melting anomaly (question marks on Fig. 3 and area located on Fig. 6). The rheology of the oceanic lithosphere of this segment appears to be modified by off-axis higher mantle temperatures, which caused the abundant volcanism, thus resulting in a thick oceanic crust and a lack of seismicity. From the gravity, magnetic and bathymetric studies, we argue that the western segment displayed voluminous melt supply since at least the A5 epoch. The most intense magmatic activity is located in the southern flank of the segment #1 at  $13^{\circ}20'N$  latitude, where we suggest the presence of a local melting anomaly. Opposite eastward and westward propagations originate from this melting anomaly, and persist during the maximum pulse of the corresponding magmatic activity (between A5 and A4a). The magnetic data show a strong asymmetry between A5c and A5 (16–11 Ma), with the northern flank wider than the southern flank (Figs 3 and 6). We can use the best-fitting synthetic magnetic profile to explain this asymmetry, since the magnetic sequences provide evidence for a ridge jump towards the south just before A5, with a half spreading rate of  $11 \text{ mm yr}^{-1}$  (Fig. 3). Spreading asymmetries are mainly caused by ridge propagation towards the mantle plume or minor ridge jumps, sustained by asthenospheric flow leading to voluminous dyke intrusion on the ridge flank proximal to the hotspot (e.g. Müller *et al.* 1998). Global positioning system (GPS) plate models indicate that Arabia is moving  $N40^{\circ}E$  at an average rate of  $22 \text{ mm yr}^{-1}$  (Reilinger *et al.* 1997; McClusky *et al.* 2000; Sella *et al.* 2002). Assuming that the positive topographic anomaly and the negative residual anomaly mark the present location of the melting anomaly at  $13^{\circ}20'N$  latitude, the present-day distance from the ridge to the thermal anomaly is 140 km (Fig. 6). After A5, the half spreading rate appears symmetrical, and no ridge jump is recorded (Fig. 3). Mittelstaedt *et al.* (2008) showed that ridge jumps could only occur in young and slow moving lithosphere. The Sheba ridge is migrating away from the  $13^{\circ}20'N$  melting anomaly while maintaining a connecting flow to the active ridge, as observed in the Galapagos/Cocos Ridge (Morgan 1978; Schilling *et al.* 1982; Ito

et al. 1997), the Reunion/Central Indian Ridge (Morgan 1978) and the Ascension/South Atlantic Ridge (Hanan et al. 1985; Schilling et al. 1985). Thus, the most plausible model appears to be a recent local melting anomaly enhanced by the edge effect of the AFTF and the close continental margins.

The oceanic crust close to the conjugate margins is thicker in the western than in the eastern domain. Hence, the two oceanic domains have remained distinct since the initiation of the ocean–continent transition. In the ocean–continent transition of the eastern domain, gravity models indicate highly thinned crust, while the seismic and magnetic data suggest the predominance of tectonic rather than magmatic processes. Moreover, the presence of non-oceanic magnetic anomalies could indicate a crust made up of exhumed serpentinized mantle (d'Acremont et al. 2006). The influence of the melting anomaly began to be felt after the continental breakup, as the margins show no evidence of excessive rifting-stage volcanism (d'Acremont et al. 2005; Autin et al. 2009; Lucazeau et al. 2009), and appears to have mainly occurred after A5, since thicker oceanic crust was formed at that time. Moreover, recent deep thermal anomaly is observed below the margins (Lucazeau et al. 2008; Basuzau et al. 2009). In addition, geophysical observations and whole-rock analyses carried out between the Afar plume and the study area support the existence of recent magmatic activity and a low velocity anomaly as far as longitude 54°E (Leroy et al. 2009b). Given the possible effect of the young oceanic basin configuration and structure on plume material distribution, Leroy et al. (2009b) propose a channelized flow model of plume–ridge interaction along the Aden and Sheba ridges, in relation to the Afar plume. According to this interpretation, the influence of the plume may extend eastward up to the Encens–Sheba area.

## 7.2 The Alula–Fartak and Socotra–Hadbeen transform faults: plate readjustment

Offsets on the continental shelf of Somalia and Yemen indicate that the AFTF and the SHTF shift the conjugate continental margins (Fig. 1). Onshore and offshore structural studies show that the AFTF and SHTF formed during the emplacement of the ocean–continent transition just after the rifting episode (d'Acremont et al. 2006; Taylor et al. 2009). Multibeam and gravity coverage reveals the complex structure of the AFFZ and SHFZ (Fig. 7).

The AFTF is not characterized by a single narrow transform valley, but by two subparallel 180-km long troughs, 10 km wide on average, joining the two offset segments of the Sheba and Aden ridges (Fig. 7). To explain both the width and the structural pattern of the transform fault zone, we propose that a mid-transform spreading axis is initiating at mid-length of the AFTF, at 14°N latitude, where the two troughs join (Fig. 7Ab). The magnetic profile S, running across the AFTF, indicates two symmetric peaks around a low centred at 14°N (Fig. 7Aa). This low could be interpreted as the signature of the new ridge axis (Fig. 7Aa). 3-D finite element simulations with realistic brittle rheology show that the lithosphere generates a region of enhanced mantle upwelling and elevated temperatures along the transform (Behn et al. 2007). The highest temperatures and thinnest lithosphere are predicted to be near the centre of the transform, where we propose the creation of a new ridge axis.

The active motion on the southern mid-length sector of the transform fault is concentrated within the narrow deep western trough. In the northern mid-length sector, an extensional relay zone shifts the transform fault on the steep eastern wall. On the eastern flank of the steep northern wall, the crustal thickness map indicates an elongated mass deficit with thick (or low density) crust; as seen on the

southern–western flank, this feature marks the present-day active transform boundary (Fig. 7Aa). The strike of the two active fault zones trends approximately N25°, while the old fracture zones have a N30° trend (Fig. 7Ab). These observations are compatible with the classical opening change hypothesized by Menard & Atwater (1969), who propose that the mid-transform axis is developed in a transform valley widened by oblique slip. The oblique suspended valley, located west of the eastern ridge, is probably the expression of a fracture zone following the trace of the old transform offset.

Near the Oman shelf, the 25 km-width SHFZ also implies an extensional episode (Fig. 7Bb). These observations are in general agreement with those of Tamsett & Searle (1990) in the AFTF, and are comparable with the Tamayo and Siqueiros Transform Faults (Kastens et al. 1979; Pockalny et al. 1997). The counter-clockwise rotation results in a 'leaky' transform fault and the intrusion of a large and continuous transform ridge.

The structure of the AFTF and SHFZ could be attributed to extension resulting from a change in kinematic regime. Transform fault zones may migrate in time and space, and this migration can be accommodated by the development of strike-slip tectonics, (e.g. compressional and/or extensional relay zones, secondary structures, etc.). In the course of time, this may create a tectonized transform zone varying both in width and structural style along strike (Gallo et al. 1986). The spreading direction has recently rotated counter-clockwise, from N30° to N025° (Fig. 7Ab). The initiation of significant extension across the transform faults creates wide basins trending N025°.

This opening of the transforms was probably initiated recently in response to a regional readjustment of plate velocities and directions: (1) an increase in the rate of opening of the East-African Rift, 3.5 Ma ago (Girdler et al. 1969; Tamsett & Searle 1990; Eagles et al. 2002; Calais et al. 2003). (2) opening of the Red Sea, with onset of seafloor spreading in the southern Red Sea at 4 Ma (e.g. Cochran 1983) and seafloor spreading jumps to the west of the Danakil microplate (Barberi & Varet 1977; Oppenheimer & Francis 1998). (3) The absolute motion of the African Plate changed between 8 and 4 Ma (Pollitz 1991). (4) Kinematic reorganization occurred in the Indian Ocean 8 Ma (Merkouriev & DeMets 2006), leading to a change in configuration of the Arabia–India–Africa triple junction (Fournier et al. 2007).

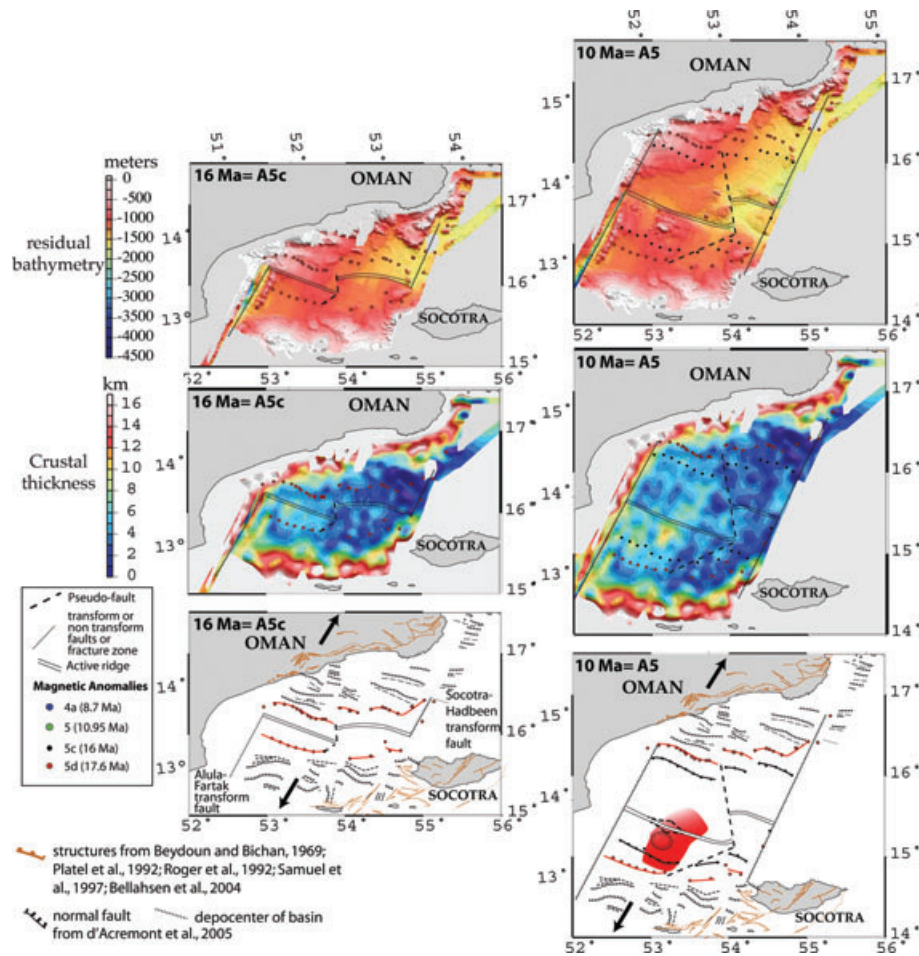
## 7.3 Evolution of segmentation

Table 1 reports the finite rotation parameters used in this study. To investigate the evolution of the segmentation of the Sheba Ridge, we interpret the magnetic anomalies and crustal thicknesses observed on both flanks of the spreading centre. Fig. 10 shows the palaeo-positions of the residual topography and the crustal thickness at A5c (16 Ma), A5 (11 Ma), A4a (9 Ma) and A3a (6 Ma).

*From A5d:* The segmentation of the initial oceanic spreading centre, which is dated at least at 17.6 Ma by A5d, is related to the structural geometry of the margins. The development of segmentation is very rapid following the continental breakup. After the

**Table 1.** Arabia–Somalia Finite Rotations used in Fig. 10.

Anomaly numbers	Age (Ma)	Latitude (°N)	Longitude (°E)	$w$ (°)
3a	5.890	22.9	27.4	2.56
4a	8.699	22.9	27.4	3.96
5	10.949	23.5	27.4	4.81
5c	16.014	24.46	27.41	7.31



**Figure 10.** Development of segmentation in the oceanic basin of the eastern Gulf of Aden from 16 to 6 Ma (A5c to A3a). (a) from A5c to A5. (b) from A4a to A3a. Top panel: Residual bathymetry (subsidence with age corrected). Middle panel: Map of crustal thickness. Bottom panel: Schematic evolution of ridge segmentation. Red and pink zones indicate volcanic areas. Black solid arrows show the plate motion, white arrows show the distensive component.

initiation of seafloor spreading, thicker crust and voluminous volcanic products are present east of the AFTF in segment #1, whereas thinner crust and reduced volcanic activity are suggested in discontinuities associated with the smaller offsets of segments #2, 3 and 4 (Figs 4d and 8). A large propagator is active from A5d to A4a (Figs 10a and b). There is evidence of a V-shaped pseudo-fault geometry, typical of spreading centre propagation, which delimits the abnormally thick oceanic crust around segment #1. The western segment #1 propagates eastwards, thus reducing the size of the central segment, which subsequently disappears. The propagating ridge curves into the offset and defines an overlap zone about 20 km long.

*From A5:* Around 11 Ma, the melting anomaly leads to a southward ridge jump. This southern anomaly at 13°20'N suggests local differences in thermal state, which control a rapid propagation eastward and westward away from the centre of the palaeo-spreading segment #1.

*From A4a:* The propagators are inferred to have ceased after A4a (9 Ma), when the magmatism appears less intense and focused, associated with a change in the boundary conditions beginning at about 8 Ma (Pollitz 1991; Merkouriev & DeMets 2006; Fournier *et al.* 2007). From this time onward, a transform fault bounds the western limit of the segment #3 (STF), and a third segment (#2) is created. Finally, a component of opening across the AFTF and SHFZ is initiated at around 9–6 Ma (Fig. 7).

The propagation of ridge segments, along with the development of transient segments, produces rift jumps towards the plume and, as a result, a large offset of the transform faults. This mechanism has already been observed in other cases of interaction between plumes and migrating mid-ocean ridges (e.g. Schilling 1991).

## 8 CONCLUSIONS

A melt pulse causes rift propagation and a rift jump shortly after the onset of seafloor spreading. We propose that a melting anomaly developed at latitude 13°20'N, leading to a ridge jump just before A5. Moreover, recent tectonic changes (around 9–6 Ma) caused the formation of transform faults and produced the pull-apart basins of AFTF and SHFZ.

The geophysical data show that the contrasts in depth and texture between the basins had been initiated by at least A5. These contrasts persist throughout the subsequent spreading history, according to the geometry of the major eastward propagator. However, differences are observed in the magmatic signatures following the continental breakup, with more intense activity occurring in the western compared with the eastern basin. The melt supply reached a climax at around 11 Ma (A5).

The traces of discontinuities, as well as the magnetic anomalies and the pattern of crustal thickness variations calculated from gravity data, suggest that the ocean–continent transition and the

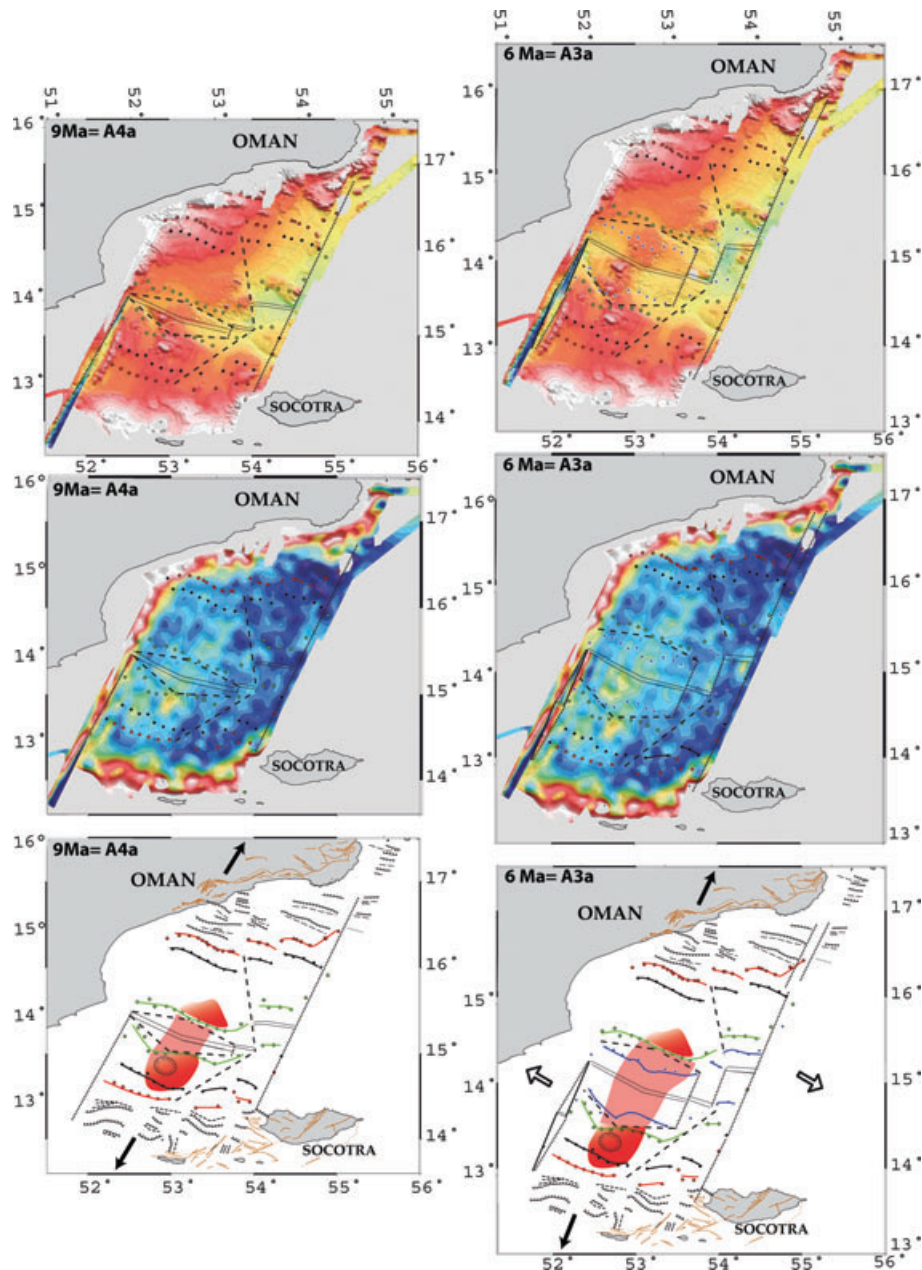


Figure 10 (Continued.)

initial oceanic spreading segments are related to the structure of the conjugate margins. From the onset (17.6 Ma), the segmentation evolved through time with an eastward propagation of segment #1 and a ridge jump. Both of these phenomena result from the enhanced and focused magmatic activity related to the melting anomaly and the edge effect of the AFTF and the nearby continental margins. At 11 Ma, the spreading asymmetry between A5c and A5 shows a ridge jump towards the southern melting anomaly, associated with the propagation of palaeo-segment #1. From 9 Ma, in relation to an overall kinematic change, and the decreased influence of the local melting anomaly on the ridge, the ridges ceased propagating. This is followed by the appearance of the STF and segment #2. The geological consequences of a recent kinematic change involve a counter-clockwise rotation of the stress field, a change in the trend of the AFFZ and SHFZ, and their opening according to a WNW–ESE direction. We propose that a new oceanic spreading

centre is being created through the AFTF, between the Aden ridge and the Sheba ridge.

The timing of magmatic and tectonic activity is not coordinated between adjacent spreading segments in close proximity. The western and eastern parts of the studied basin exhibit contrasting styles of seafloor spreading. The present-day active axis of segment #1 is an atypical ridge interpreted as an end-member representative of slow-spreading segments with ‘hotter-large-melt supply’.

#### ACKNOWLEDGMENTS

The work was funded by the GDR Marges–Aden project and is supported by Action Marges and ANR YOCMAL. We are deeply grateful to the officers and crew of the R/V Marion-Dufresne (IPEV) for the acquisition of the Encens–Sheba data set. We deeply thank P. Patriat who helped us to compute the magnetic anomalies model

and offered valuable comments on the manuscript. We also appreciate thoughtful and constructive reviews from R. Pockalny and an anonymous reviewer. S. Mercouriev and P. Styles kindly provided us with the data from ug78 and sk79 magnetic profiles, respectively. We also thank Dr Hilal Al-Azri, S. Al Busaïdi and A. Al-Khatiri from the Directorate of Minerals of Oman for their help, both on-board ship and for administrative assistance. We also thank Dr K. Khanbari, A. Al-Subbary and Dr Al Ganad for their assistance with the work in Yemeni waters. Dr M.S.N. Carpenter post-edited the English style.

## REFERENCES<sup>1</sup>

- Autin, J. *et al.*, 2009. Continental breakup history of a deep-magma poor margin from seismic reflection data (northeastern Gulf of Aden margin, offshore Oman), *Geophys. J. Int.*, in press, doi:10.1111/j.1365-246X.2009.04424.x (this issue).
- Barberi, F. & Varet, J., 1977. Volcanism of Afar: smallscale plate tectonic implications, *Geol. Soc. Am. Bull.*, **56**, 903–915.
- Basayau, C., Tiberi, C., Leroy, S., Stuart, G., Al-Lazki, A., Al-Toubi, K. & Ebinger, C., 2009. Evidence of political melting beneath a continental margin: case of Dhofar, in the Northeast Gulf of Aden (Sultanate of Oman), *Geophys. J. Int.*, in press, doi:10.1111/j.1365-246X.2009.04438.x (this issue).
- Behn, M.D., Boettcher, M.S. & Hirth, G., 2007. Thermal structure of oceanic transform faults, *Geology*, **35**, 307–310.
- Bellahsen, N., Fournier, M., d'Acremont, E., Leroy, S. & Daniel, J.M., 2006. Fault reactivation and rift localization: the northeastern Gulf of Aden margin, *Tectonics*, **25**, doi:10.1029/2004TC001626.
- Beydoun, Z.R. & Bichan, H.R., 1969. The geology of Socotra Island, Gulf of Aden, *Quat. J. Geol. Soc. London*, **125**, 413–446.
- Birse, A.C.R., Bott, W.F., Morrison, J. & Samuel, M.A., 1997. The Mesozoic and Early Tertiary Tectonic Evolution of the Socotra Area, Eastern Gulf of Aden, Yemen, *Mar. Petrol. Geol.*, **14**, 673–683.
- Bonatti, E., 1978. Vertical tectonism in oceanic fracture zones, *Earth planet. Sci. Lett.*, **37**, 369–379.
- Brannan, J., Gerdes, K.D. & Newth, I.R., 1997. Tectono-stratigraphic development of the Qamar basin, Eastern Yemen, *Mar. Pet. Geol.*, **14**, 701–730.
- Briais, A., Aslanian, D., Géli, L. & Ondréas, H., 2002. Analysis of propagators along the Pacific-Antarctic Ridge: evidence for triggering by kinematic changes, *Earth planet. Sci. Lett.*, **199**, 415–428.
- Calais, E., DeMets, C. & Nocquet, J.-M., 2003. Evidence for post-3.16 Ma change in Nubia-Eurasia-North America plate motions, *Earth planet. Sci. Lett.*, **216**, 81–92.
- Cande, S.C. & Kent, D.V., 1995. Revised calibration of the geomagnetic polarity timescale for the Late Cretaceous and Cenozoic, *J. geophys. Res.*, **100**, 6093–6095.
- Cannat, M., 1993. Emplacement of Mantle rocks in the Seafloor at Mid-Ocean Ridges, *J. geophys. Res.*, **98**, 4163–4172.
- Cochran, J.R., 1982. The magnetic quiet zone in the eastern Gulf of Aden: implications for the early development of the continental margin, *Geophys. J. Int.*, **68**, 171–201.
- Cochran, J.R., 1983. A model for the development of the Red Sea, *Am. Assoc. Pet. Geol. Bull.*, **67**, 41–69.
- Courtilot, V., 1980. Opening of the Gulf of Aden and Afar by progressive tearing, *Phys. Earth planet. Inter.*, **21**, 343–350.
- d'Acremont, E., Leroy, S., Beslier, M.O., Bellahsen, N., Fournier, M., Robin, C., Maia, M. & Gente, P., 2005. Structure and evolution of conjugate passive margins of the eastern gulf of Aden from seismic reflection data, *Geophys. J. Int.*, **160**, 869–890.
- d'Acremont, E., Leroy, S., Maia, M., Patriat, P., Beslier, M.O., Bellahsen, N., Fournier, M. & Gente, P., 2006. Structure and evolution of the eastern Gulf of Aden: insights from magnetic and gravity data (Encens-Sheba cruise), *Geophys. J. Int.*, **165**, 786–803.
- Dauteuil, O., Huchon, P., Quemeneur, F. & Souriot, T., 2001. Propagation of an oblique spreading center: the western Gulf of Aden, *Tectonophysics*, **332**, 423–442.
- Davis, E.E. & Lister, C.R.B., 1974. Fundamentals of ridge crest topography, *Earth planet. Sci. Lett.*, **21**, 405–413.
- DeMets, C., Gordon, R.G., Argus, D.F. & Stein, S., 1990. Current plate motions, *Geophys. J. Int.*, **101**, 425–478.
- DeMets, C., Gordon, R.G. & Vogt, P., 1994. Location of the Africa-Australia-India triple junction and motion between Australian and Indian plates: results from an aeromagnetic investigation of the Central Indian and Carlsberg ridges, *Geophys. J. Int.*, **119**, 895–930.
- Detrick, R.S., Needham, H.D. & Renard, V., 1995. Gravity anomalies and crustal thickness variations along the Mid-Atlantic Ridge between 33°N and 40°N, *J. geophys. Res.*, **100**, 3767–3787.
- Eagles, G., Gloaguen, R. & Ebinger, C., 2002. Kinematics of the Danakil microplate, *Earth planet. Sci. Lett.*, **203**, 607–620.
- Ebinger, C.J. & Hayward, N.J., 1996. Soft plates and hot spots: views from Afar, *J. geophys. Res.*, **101**, 21 859–21 876.
- Escartin, J. & Cannat, M., 1999. Ultramafic exposures and the gravity signature of the lithosphere near the Fifteen-Twenty Fracture Zone (Mid-Atlantic Ridge, 14°–16.5°N), *Earth planet. Sci. Lett.*, **171**, 411–424.
- Fisher, R.L., Bunce, E.T. & the scientific team, 1974. Sites. in *Initial Reports of the Deep Sea Drilling Project*, pp. 231–238, 24, ed. Musich, L., U.S. Government Printing Office, Washington.
- Fleury, J.M., 2001. Cinématique de la frontière Somalie-Arabie et ouverture du Golfe d'Aden, IGP, Mémoire de DEA, Paris.
- Fournier, M., Patriat, P. & Leroy, S., 2001. Reappraisal of the Arabia-India-Somalia triple junction kinematics, *Earth planet. Sci. Lett.*, **189**, 103–114.
- Fournier, M., Chamot-Rooke, N., Petit, C., Fabbri, O., Huchon, P., Maillot, B. & Lepvrier, C., 2007. In situ evidence for dextral active motion at the Arabia-India plate boundary, *Nat. Geosci.*, **1**, 54–58.
- Fournier, M., Petit, C., Chamot-Rooke, N., Fabbri, O., Huchon, P., Maillot, B. & Lepvrier, C., 2008. Do ridge-ridge-fault triple junctions exist on Earth? Evidence from the Aden-Owen-Carlsberg junction in the NW Indian Ocean, *Basin Res.*, **20**, 575–590.
- Fox, P.J. & Gallo, D.G., 1984. A tectonic model for ridge-transform-ridge plate boundaries: implication for the structure of oceanic lithosphere, *Tectonophysics*, **104**, 205–242.
- Fox, P.J. & Grindlay, N.R., 1991. The Mid-Atlantic Ridge (31°S–34°30'S): temporal and spatial variations of accretionary processes, *Mar. geophys. Res.*, **13**, 1–20.
- Gallo, D.G., Fox, P.J. & Macdonald, K.C., 1986. A sea beam investigation of the clipperton transform fault: the morphotectonic expression of a fast slipping transform boundary, *J. geophys. Res.*, **91**, 3455–3467.
- Gente, P. *et al.*, 1995. Characteristics and evolution of the segmentation of the Mid-Atlantic Ridge between 20°N and 24°N during the last 10 million years, *Earth planet. Sci. Lett.*, **129**, 55–71.
- Gente, P. *et al.*, 2001. The SHEBA ridge: a particular spreading center or an end-member of the slow spreading processes? *AGU Fall Meeting*, suppl. EOS, 1251.
- Gente, P., Leroy, S., Maia, M., Blais, A., d'Acremont, E. & Patriat, P., 2003. The high magmatic budget of one SHEBA ridge segment: an End-member of the slow spreading processes, *Geophys. Res. Abs., EGS-AGU-EUG Joint Assembly*, **5**, 14 830.
- Girdler, R.W., Fairhead, J.D., Searle, R.C. & Sowerbutts, W.T.C., 1969. Evolution of rifting in Africa, *Nature*, **224**, 1178–1182.
- Grindlay, N.R., Fox, P.J. & Vogt, P.R., 1992. Morphology and tectonics of the Mid-Atlantic Ridge (25°–27°30'S) from sea beam and magnetic data, *J. geophys. Res.*, **97**, 6983–7010.
- Hanan, B.B., Kingsley, R.H. & Schilling, J.G., 1985. Pb isotope evidence in the South Atlantic for migrating ridge-hotspot interactions, *Nature*, **322**, 137–144.
- Hébert, H., Deplus, C., Huchon, P., Khanbari, K. & Audin, L., 2001. Lithospheric structure of a nascent spreading ridge inferred from gravity data: the western Gulf of Aden, *J. geophys. Res.*, **106**, 26 345–26 363.

<sup>1</sup>Correction after online publication 2009 December 24: missing references have been added to this list.

- Hooft, E.E.E., Detrick, R.S., Toomey, D.R., Collins, J.A. & Lin, J., 2000. Crustal thickness and structure along three contrasting spreading segments of the Mid-Atlantic Ridge, 33.5°–35°N, *J. geophys. Res.*, **105**, 8205–8226.
- Ito, G., Lin, J. & Gable, C.W., 1997. Interaction of mantle plumes and migrating mid-ocean ridges: implications for the Galapagos plume-ridge system, *J. geophys. Res.*, **102**, 15 403–15 417.
- Jestin, F., Huchon, P. & Gaulier, J.M., 1994. The Somalia plate and the East African Rift System: present-day kinematics, *Geophys. J. Int.*, **116**, 637–654.
- Kastens, K.A., Macdonald, K.C. & Becker, K., 1979. The Tamayo transform fault in the mouth of the Gulf of California, *Mar. geophys. Res.*, **4**, 129–151.
- Kuo, B.Y. & Forsyth, D.W., 1988. Gravity anomalies of the ridge-transform system in the South Atlantic between 31 and 34.5°S: upwelling centers and variations in crustal thickness, *Mar. geophys. Res.*, **10**, 205–232.
- Laughton, A.S. & Tramontini, C., 1969. Recent studies of the crustal structure in the Gulf of Aden, *Tectonophysics*, **8**, 359–375.
- Lepvrier, C., Fournier, M., Bérard, T. & Roger, J., 2002. Cenozoic extension in coastal Dhofar (southern Oman): Implications on the oblique rifting of the Gulf of Aden, *Tectonophysics*, **357**, 279–293.
- Leroy, S., Gente, P., Fournier, M. & the scientific team (d'Acremont, E., Bellahsen, N., Beslier, M.O., Patriat, P., Perrot, J., Al-Kathiri, A., Blais, A., Merkouriev, S.), 2000. Données et résultats préliminaires de la campagne MD117 ENCENS-SHEBA, IPEV published report, 87.
- Leroy, S. et al., 2004. From rifting to spreading in the eastern Gulf of Aden: a geophysical survey of a young oceanic basin from margin to margin, *Terra nova*, **16**, 185–192.
- Leroy, S. et al., 2009a. Contrasted styles of margins in the eastern Gulf of Aden, *Geochem., Geophys. Geosyst.*, submitted.
- Leroy, S., d'Acremont, E., Tiberi, C., Basuyau, C., Autin, J. & Lucazeau, F., 2009b. Recent off-axis volcanism in the eastern Gulf of Aden: implications for plume-ridge interaction, *Earth planet. Sci. Lett.*, submitted.
- Lin, J., Purdy, G.M., Schouten, H., Sempere, J.C. & Zervas, C., 1990. Evidence from gravity data for focused magmatic accretion along the Mid-Atlantic Ridge, *Nature*, **344**, 627–632.
- Lonsdale, P., 1994. Structural geomorphology of the Eltanin fault system and adjacent transform faults of the Pacific-Antarctic Plate Boundary, *Mar. geophys. Res.*, **16**, 105–143.
- Lucazeau, F. et al., 2008. Persistent thermal activity at the Eastern Gulf of Aden after continental break-up, *Nat. Geosci.*, **1**, 854–858.
- Lucazeau, F. et al., 2009. Post-rift volcanism and high heat-flow at the ocean–continent transition of the eastern Gulf of Aden, *Terra nova*, **21**, 285–292.
- Macdonald, K.C., 1982. Mid-ocean ridges: fine scale tectonic, volcanic and hydrothermal processes within the plate boundary zone, *Annu. Rev. Earth planet. Sci.*, **10**, 155–190.
- Macdonald, K.C., Scheirer, D.C. & Carbotte, S.M., 1991. Mid-ocean ridges: discontinuities, segments and giant cracks, *Science*, **253**, 986–994.
- Magde, L.S. & Sparks, D.W., 1997. Three-dimensional mantle upwelling, melt generation, and melt migration beneath segment slow spreading ridges, *J. geophys. Res.*, **102**, 20 571–20 583.
- Maia, M. & Arkani-Hamed, J., 2002. The support mechanism of the young Foundation Seamounts inferred from bathymetry and gravity, *Geophys. J. Int.*, **149**, 190–210.
- Maia, M. & Gente, P., 1998. Three-dimensional gravity and bathymetry analysis of the Mid-Atlantic Ridge between 20°N and 24°N: flow geometry and temporal evolution of the segmentation, *J. geophys. Res.*, **103**, 951–974.
- Manighetti, I., Tapponnier, P., Gillot, P.Y., Jacques, E., Courtillot, V., Armijo, R., Ruegg, J.C. & King, G., 1998. Propagation of rifting along the Arabia-Somalia plate boundary: into Afar, *J. geophys. Res.*, **103**, 4947–4974.
- Martinez, F., Taylor, B. & Goodliffe, A.M., 1999. Contrasting styles of seafloor spreading in the Woodlark Basin: indications of rift-induced secondary mantle convection, *J. geophys. Res.*, **104**, 12 909–12 926.
- McClusky, S.C., Balassanian, S., Barka, A., Demir, C., Ergintav, S. et al., 2000. Global Positioning System constraints on plate kinematics and dynamics in the eastern Mediterranean and Caucasus, *J. geophys. Res.*, **105**, 5695–5719.
- Menard, H.W. & Atwater, T., 1969. Origin of Fracture Zone Topography, *Nature*, **222**, 1037–1040.
- Menzies, M.A., Gallagher, K., Yelland, A. & Hurford, A., 1997. Volcanic and nonvolcanic rifted margins of the Red Sea and Gulf of Aden: crustal cooling and margin evolution in Yemen, *Geochem. Cosmochim. Acta.*, **61**, 2511–2527.
- Merkouriev, S. & DeMets, C., 2006. Constraints on Indian plate motion since 20 Ma from dense Russian magnetic data: implications for Indian plate dynamics, *Geochem. Geophys. Geosyst.*, **7**, Q02002, doi:10.1029/2005GC001079.
- Mittelstaedt, E., Ito, G. & Behn, M.D., 2008. Mid-ocean ridge jumps associated with hotspot magmatism, *Earth planet. Sci. Lett.*, **266**, 256–270.
- Morgan, W.J., 1978. Rodriguez, Darwin, Amsterdam... a second type of hotspot island, *J. geophys. Res.*, **85**, 5355–5360.
- Morris, E. & Detrick, R.S., 1991. Three-dimensional analysis of gravity anomalies in the MARK area, Mid-Atlantic ridge 23°N, *J. geophys. Res.*, **96**, 4355–4366.
- Müller, R.D., Roest, W.R. & Royer, J.Y., 1998. Asymmetric sea-floor spreading caused by ridge-plume interactions, *Nature*, **396**, 455–459.
- Niu, Y., Bideau, D., Hékinian, R. & Batiza, R., 2001. Mantle compositional control on the extent of mantle melting, crust production, gravity anomaly, ridge morphology, and ridge segmentation: a case study at the Mid-Atlantic Ridge 33–35°N, *Earth planet. Sci. Lett.*, **186**, 383–399.
- Oppenheimer, C. & Francis, P., 1998. Implications of longeval lava lakes for geomorphological and plutonic processes at Erta 'Ale volcano, Afar, *J. Volc. Geother. Res.*, **80**, 101–111.
- Parsons, B. & Sclater, J.G., 1977. An analysis of the variation of ocean floor bathymetry and heat flow with age, *J. geophys. Res.*, **82**, 803–827.
- Phipps Morgan, J.P. & Forsyth, D.W., 1988. Three-dimensional flow and temperature perturbations due to a transform offset: effects on oceanic crustal and upper mantle structure, *J. geophys. Res.*, **93**, 2955–2966.
- Platel, J.P. & Roger, J., 1989. Evolution géodynamique du Dhofar (Sultanat d'Oman) pendant le Crétacé et le Tertiaire en relation avec l'ouverture du golfe d'Aden, *Bull. Soc. géol. France*, **2**, 253–263.
- Platel, J.P., Roger, J., Peters, T.J., Mercolli, I., Kramers, J.D. & Le Métour, J., 1992. Geological map of Salalah, Sultanate of Oman; sheet NE 40–09, eds Platel, J.P., Roger, J., Peters, T.J., Mercolli, I., Kramers, J.D. & Le Métour, J., Ministry of Petroleum and Minerals, Directorate General of Minerals, Oman.
- Pockalny, R., 1997. Evidence of transpression along the Clipperton Transform: implications for processes of plate boundary reorganization, *Earth planet. Sci. Lett.*, **146**, 449–464.
- Pockalny, R.A., Gente, P. & Buck, R., 1996. Oceanic transverse ridges: a flexural response to fracture-zone-normal extension, *Geology*, **24**, 71–74.
- Pockalny, R.A., Fox, P.J., Fornari, D.J., Macdonald, K.C. & Perfit, M.R., 1997. Tectonic reconstruction of the Clipperton and Siqueiros fracture zones: evidence and consequences of plate motion changes for the last 3 Myr, *J. geophys. Res.*, **102**, 3167–3181.
- Pollitz, F.F., 1991. Two-stage model of African absolute motion during the last 30 million years, *Tectonophysics*, **194**, 91–106.
- Potts, C.S., White, R.S. & Loudon, K.E., 1986. Crustal structure of Atlantic fracture zones—II. The Vema fracture zone and transverse ridge, *Geophys. J. R. astr. Soc.*, **86**, 491–513.
- Rabain, A., Cannat, M., Escartin, J., Pouliquen, G., Deplus, C. & Rommevaux-Jestin, C., 2001. Focused volcanism and growth of a slow spreading segment (Mid-Atlantic Ridge, 35°N), *Earth planet. Sci. Lett.*, **185**, 211–224.
- Reilinger, R.E. et al., 1997. Global Positioning System measurements of present-day crustal movements in the Arabia-Africa-Eurasia plate collision zone, *J. geophys. Res.*, **102**, 9983–9999.
- Roger, J., Platel, J.P., Cavelier, C. & Grisac, C.B.D., 1989. Données nouvelles sur la stratigraphie et l'histoire géologique du Dhofar (Sultanat d'Oman), *Bull. Soc. géol. France*, **V**, 265–277.
- Rommevaux, C., Deplus, C., Patriat, P. & Sempéré, J.C., 1994. Three-dimensional gravity study of the Mid-Atlantic Ridge: evolution of the

- segmentation between 28° and 29°N during the last 10 m.y., *J. geophys. Res.*, **99**, 3015–3029.
- Sandwell, D.T. & Smith, W.H.F., 1997. Marine gravity anomaly from Geosat and ERS1 satellite altimetry, *J. geophys. Res.*, **102**, 10 039–10 054.
- Sauter, D., Patriat, P., Rommevaux-Jestin, C., Cannat, M., Briais, A. & Gallieni Shipboard Scientific Party, 2001. The Southwest Indian Ridge between 49°15'E and 57°E: focused accretion and magma redistribution, *Earth planet. Sci. Lett.*, **192**, 303–317.
- Schilling, J.G., 1973. Afar mantle plume: rare earth evidence, *Nature*, **242**, 2–5.
- Schilling, J.G., 1991. Fluxes and excess temperatures of mantle plumes inferred from their interaction with migrating mid-ocean ridges, *Nature*, **352**, 397–403.
- Schilling, J.G., Kingsley, R.H. & Devine, J.D., 1982. Galapagos hot spot-spreading center system, 1, Spatial petrological and geochemical variations (83°W–101°W), *J. geophys. Res.*, **87**, 5593–5610.
- Schilling, J.G., Thompson, G., Kingsley, R.H. & Humphris, S., 1985. Hotspot-migrating ridge interaction in the South Atlantic, *Nature*, **313**, 187–191.
- Schouten, H., Klitgord, K.D. & Whitehead, J.A., 1985. Segmentation of mid-ocean ridges, *Nature*, **317**, 225–229.
- Schouten, H., Dick, H.J.B. & Klitgord, K.D., 1987. Migration of mid-ocean ridges, *Nature*, **326**, 835–839.
- Sella, G.F., Dixon, T.H. & Mao, A.L., 2002. REVEL: a model for recent plate velocities from space geodesy, *J. geophys. Res.*, **107**, 2081.
- Sempéré, J.-C., Lin, J., Brown, H.S., Schouten, H. & Purdy, G.M., 1993. Segmentation and morphotectonic variations along a slow spreading center: the Mid-Atlantic Ridge (24°00'N–30°40'N), *Mar. geophys. Res.*, **15**, 153–200.
- Sparks, D.W., Parmentier, E.M. & Phipps Morgan, J., 1993. Three-dimensional mantle convection beneath a segmented spreading center; implications for along-axis variations in crustal thickness and gravity, *J. geophys. Res.*, **98**, 21 977–21 995.
- Supak, S., Carbotte, S. & Macdonald, K., 2007. Influence of ridge migration and proximity to hot spots on the morphology of slow- and intermediate-spreading centers, *Geochem. Geophys. Geosyst.*, **8**, 1–23.
- Tamsett, D. & Searle, R., 1990. Structure of the Alula-Fartak Fracture Zone, Gulf of Aden, *J. geophys. Res.*, **95**, 1239–1254.
- Tard, F., Masse, P., Walgenwitz, F. & Gruneisen, P., 1991. The volcanic passive margin in the vicinity of Aden, Yemen, *BCREDP (Bulletin des Centres de Recherches Exploration Production)*, **15**, 1–9.
- Taylor, B., Goodliffe, A. & Martinez, F., 2009. Initiation of transform faults at rifted continental margins, *C. R. Geosci.*, **341**, 428–438.
- Thibaud, R., Gente, P. & Maia, M., 1998. A systematic analysis of the morphology and the gravity along the Mid-Atlantic Ridge between 15°N and 40°N: constrains for the thermal structure, *J. geophys. Res.*, **103**, 24 223–24 243.
- Tucholke, B.E. & Lin, J., 1994. A geological model for the structure of ridge segments in slow-spreading ocean crust, *J. geophys. Res.*, **99**, 11 937–11 958.
- Wessel, P. & Smith, W.H.F., 1998. New improved version of Generic Mapping Tools released, *EOS, Trans. Am. Geophys. Un.*, **79**, 579.